UNIVERSITY OF CALIFORNIA, SAN DIEGO

The Electric Sense of the Thornback Ray, *Platyrhinoidis triseriata*: Linear Dynamic Range in Single-Unit Electrophysiological Recordings *in vivo* from the Afferent Nerve Fibers of the Ampullae of Lorenzini

A dissertation submitted in partial satisfaction of the
requirements for the degree Doctor of Philosophy
in
Oceanography

by

Ivan F. Gonzalez

Committee in charge:

Adrianus J. Kalmijn, Co-Chair
John A. Hildebrand, Co-Chair
William S. Hodgkiss
Robert Pinkel
Terrence J. Sejnowski

2008

The dissertation of Ivan F. Gonzalez is approved, and it is acceptable in quality and form for publication on microfilm:

Co-Chair

Co-Chair

University of California, San Diego

2008

DEDICATION

To the sea, to family, to love

EPIGRAPH

Wonderful as are the laws and phenomena of electricity when made evident to us in inorganic or dead matter, their interest can bear scarcely any comparison with that which attaches to the same force when connected with the nervous system and with life.

Michael Faraday

TABLE OF CONTENTS

LIST OF FIGURES

LIST OF TABLES

VITA

1997-1998	Teaching Assistant, Physics Department, Universidad de Los Andes, Colombia
1998	B.S. (Fisico), Universidad de Los Andes, Colombia
2000	Internship in electrophysiological techniques, Laboratorio de Neurofarmacologia celular, IVIC, Venezuela
2002-2003	Staff Research Associate, Sensory Biophysics Laboratory, University of California, San Diego
2003	M.S., Oceanography University of California, San Diego
2003-2004	Teaching Assistant, Linguistics Department, University of California, San Diego
2003-2006	Student Research Associate Scripps Institution of Oceanography, University of California, San Diego
2004	Sussman Fund Internship, Natural Reserve System, San Diego-La Jolla Underwater Park, San Diego
2007	Teaching Assistant, Environmental System Program, Division of Physical Sciences University of California, San Diego
2008	Ph.D, Oceanography University of California, San Diego

PUBLICATIONS

Journals

1. The physical nature of life, Journal of Physiology-Paris. A. J. Kalmijn, I. F. Gonzalez and M. C. McClune, Volume 96, Number 5, pp. 355-362, September 2002

Presentations with Abstract

1. Commonalities and differences in the use of electric and inertial sense organs by predatory fish. What difference does it make it for the nerve signals? I. F. Gonzalez, M. C. McClune and A. J. Kalmijn, Complex Dynamical Processes in Electroreceptors and Hair Cells, May 17-21, 2004, Dresden, Germany

Posters with Abstract

1. Electrical Excitation: Graded positive feedback and negative conductance. I. F. Gonzalez, M. C. McClune and A. J. Kalmijn, Neurobiology of Electrosensory Organisms, July 27th to 29th 2001, Bonn, Germany
2. Commonalities and differences in the use of electric and inertial sense organs by predatory fish. What difference does it make it for the nerve signals? I. F. Gonzalez, M. C. McClune and A. J. Kalmijn, Complex Dynamical Processes in Electroreceptors and Hair Cells, May 17-21, 2004, Dresden, Germany

Others

1. Bachelor Degree Thesis: Electrorrecepcion: Modelo Electrico de Celulas Electrorreceptoras. (An electric model of the electroreceptor cells from the Ampullae of Lorenzini), Ivan F. Gonzalez. Universidad de Los Andes, Bogota Colombia

FIELDS OF STUDY

Major Field: Applied Ocean Science

Studies in Physical Oceanography
Professors Paul Robbins and Myrl C. Hendershott

Studies in Biological Oceanography
Professor Peter Franks

Studies in Marine Chemistry
Professors Joris M. Gieskes and Ralph F. Keeling

Studies in Marine Geology
Professor Peter F. Lonsdale

Studies in Applied Mathematics
Professors William R. Young, Glenn R. Ierley, and Stefan L. Smith

Additional studies:

Studies in Analysis of Oceanographic data
Professor Robert Pinkel

Studies in Observations of Large Scale Ocean circulation
Professor Dean Roemmich

Field studies in Marine Electromagnetic Methods
Professor Steven Constable

Studies in Fluid Mechanics
Professor Clinton D. Winant

Studies in Deep Sea Biology
Professor A. Aristides Yayanos

Studies in Sensory Biophysics of Aquatic Animals
Professor Adrianus J. Kalmijn

Studies in Computational Neurobiology
Professor Terrence J. Sejnowski

Studies in Basic Neuroscience
Professors Steven A. Hillyard, and Eric Courchesne

Studies in Ion Channels
Professor Paul Slesinger

ABSTRACT OF THE DISSERTATION

The Electric Sense of the Thornback Ray, *Platyrhinoidis triseriata*:
Linear Dynamic Range in Single-Unit Electrophysiological Recordings *in vivo* from the Afferent Nerve Fibers of the Ampullae of Lorenzini

by

Ivan F. Gonzalez
Doctor of Philosophy in Oceanography
University of California, San Diego, 2008
Adrianus J. Kalmijn, Co-chair
John A. Hildebrand, Co-chair

Elasmobranch fishes use their electroreceptive organs, the Ampullae of Lorenzini, to sense DC and low-frequency electric fields in the ocean. The natural environment offers a wide range of electric field strengths, from typically less than 5 nV/cm in the rapidly falling fields a meter away from hidden prey to 500 nV/cm in the wind-driven currents of the North Atlantic. In contrast, electrophysiological recordings from the electroreceptor's afferent nerves show a limited dynamic range in response to low-frequency sinusoidal stimuli, with non-linearity starting at amplitudes only eight times the organ's sensitivity threshold.

We employ *in vivo* recordings from the hyomandibular nerve of the thornback ray, *Platyrhinoidis triseriata*, to explore the physiological mechanisms exercised by elasmobranch fishes to extend their electroreceptor's sensory dynamic range in widely ranging ambient electric field strengths. We measure the organ's nerve activity in response to DC fields, to low-frequency sinusoidal electric stimuli in the presence of various DC fields and to low-frequency sinusoidal electric stimuli of different relative orientation. When possible, we record and analyze the simultaneous activity of two nerve fibers during the experiment. We propose that the animal may extend its electroreceptor's linear dynamic range of operation by using the organ's adaptation to DC fields and directional response in combination with previously described behavioral mechanisms that modulate, and sometimes produce, the effective stimulus.

1

Introduction

1.1 Environmental changes, sensory systems and action potentials

Living creatures react and adjust to environmental changes in order to survive. Their sensory systems target specific environmental variables of high biological significance, and provide an early warning to specialized control systems such as the central nervous system.

The electric conduction in nerve cells provides a fast and reliable method to transfer information from the sense organs to the central nervous system. Nerve cells conduct electric impulses of fixed form called action potentials. The information gathered by the sense organs is encoded in the differences in arrival times of the action potentials at a central point. To react properly, the animal should be able to interpret this train of action potentials using evolution-acquired mechanisms and the experience acquired during its lifetime [26, 30].

1.2 Electrical phenomena in the oceans

The oceans are vast electrolytic volume conductors covering more than two thirds of the surface of our planet. This immense region presents a wealth of electromagnetic features. Ocean currents and tidal flows moving in the earth's magnetic field induce electric fields in the ocean, telluric phenomena in the earth's crust introduce

electric fields from below, and ionospheric circulations moving in the magnetic field of the earth introduces electric fields from above, all continuously enriching the electrical seascape intrinsic to our oceans [10, 20, 33, 49].

1.3 Electroreception in elasmobranch fishes

Some aquatic life forms are capable of extracting relevant information from their electrical environment and using it to adjust their behavior accordingly. The biologically relevant electric fields in the ocean are those carrying information useful for behaviors such as feeding, reproduction and migration [19, 30].

Elasmobranch fishes, sharks, rays and chimeras, use their electric sense to orient with respect to the ambient electric and magnetic fields, to detect other animals, such as prey, and to detect the presence of underwater objects. Elasmobranch fishes have unrivaled sensitivity to DC and low-frequency electric fields in the animal kingdom, showing behavioral responses to electric fields with very little strength (5 nV/cm) [17, 19, 20, 23, 24]. The openings exposing the sense organs to the seawater can be observed on the skin of the animal (see figure 1.1).

1.3.1 The Ampullae of Lorenzini

Sharks and rays have superior specialized electroreceptive organs, the Ampullae of Lorenzini. The ampulla is an internal sense organ; the cells in charge of the sensory transduction connect to the seawater by means of a jelly-filled canal with an opening on the skin [39, 51]. Thousands of sensory cells are located at the internal end of the Ampulla of Lorenzini in the walls of the alveoli, which are the bean-shaped, hollow surfaces forming the ampullae proper [36, 51] (see part c of figure 1.2 and figure 3.4).

The number and location of the ampullary pores of sharks and rays are species-specific, reflecting the overall species size and particular adaptations to their environment. The number of pores in selected skates ranges from 380 ($\pm$72.7) in the leopard skate, *Raja garmani*, to 1,691 ($\pm$87.5) in the larger barn-door skate, *Raja laevis* [43]. The pore distribution on the ventral and dorsal surfaces of selected skates ranges from only 48 % of the total number of pores on the ventral surface of *Raja clarkii*, to 92 % in

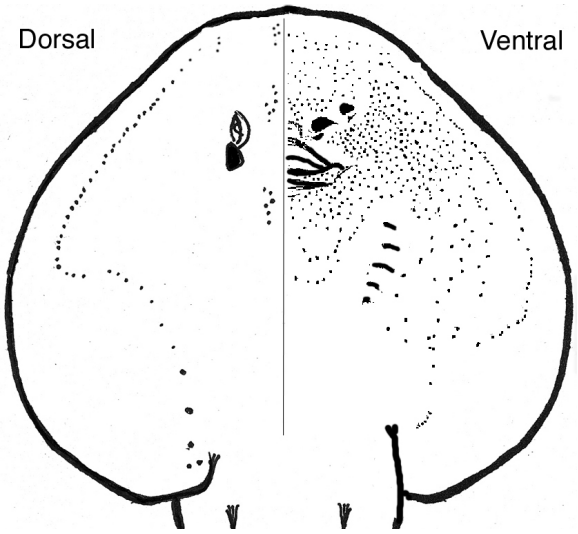

Figure 1.1: Thornback ray's ampullary pore distribution

Left side of the picture shows a diagram of pore locations on the dorsal surface. Right side shows a diagram of pore location on the ventral surface. Pores are distributed with bilateral symmetry in the animals. Modified after Montgomery [37].

Anacanthobatis longirostris [43]. The size of the animal within a species also influences the number of ampullae; a small adult Oman shark, *Iago omanensis*, may have 1,200 ($\pm$40) ampullae, while the largest females can have up to 1,800 ($\pm$70) ampullae [13].

The internal ends of the Ampullae of Lorenzini cluster in a few capsules. The capsule's wall isolates the cluster of ampullary ends from the surrounding body tissue (see figure 1.2). These capsules, distributed with left-right symmetry in the body, connect to the brain via major cranial nerves [41, 43]. Up to twenty afferent nerve fibers innervate each ampulla [2, 31, 36, 42].

1.3.2 Spontaneous activity in the ampullary nerves

The afferent nerve fibers associated with the Ampullae of Lorenzini are active even when there is no electric stimulus in the seawater. This baseline generation of nerve impulses is called the spontaneous activity of the ampulla. The spontaneous activity is characterized by a rate of action potentials per second (λ) that is nearly constant over a period of several hours.

The generation of action potentials in the ampulla's nerve fiber may be affected

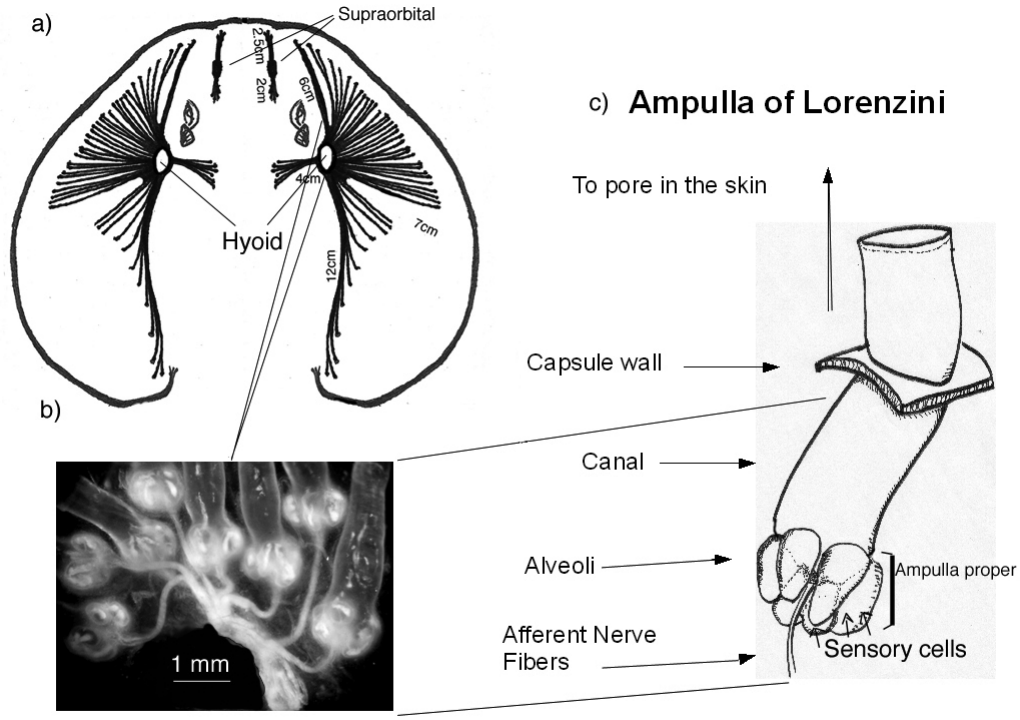

Figure 1.2: The Ampullae of Lorenzini

a) Diagram of the thornback's disc, dorsal view. Dark lines show the orientation of subcutaneous canals from the supraorbital and hyoid capsules. Canal lengths for an adult female with a 25 cm disc diameter. b) Cluster of ampullae excised from inside the hyoid capsule ($6mmX4mm$). Notice the ampulla proper (shaped as a narrow-necked, round-bodied vase) and sections of canal. Around ten afferent nerve fibers innervate each ampulla. The fibers are tightly packed together, giving the impression of being a single fiber in this picture. c) Diagram of section from the Ampulla of Lorenzini. Bottom: ampullae proper, top: canal going towards the skin. The sensory cells are located in the walls of the alveoli.

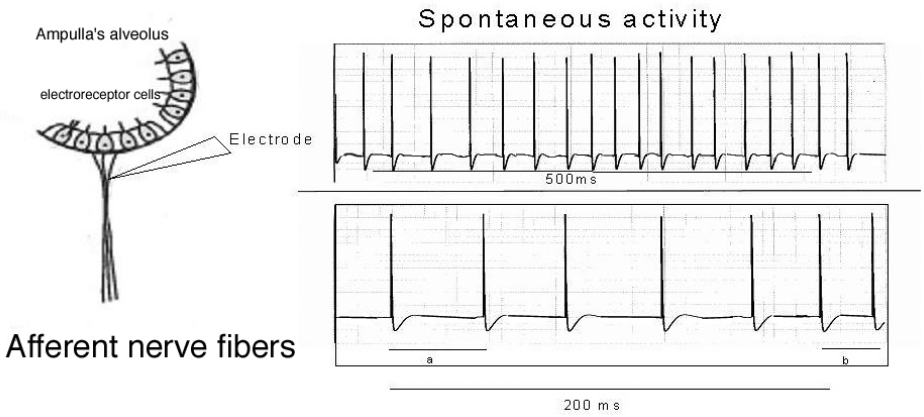

Figure 1.3: Spontaneous activity of the Ampulla of Lorenzini

Spontaneous activity of an afferent nerve from the Ampulla of Lorenzini, characterized by a regular rate of action potentials per second (λ_s). An electrode recording the spontaneous activity from a nerve fiber from the ampulla may record a train of nerve impulses similar to that shown, with 15 action potentials arriving during a 500-ms interval, representing a nerve fiber with a $\lambda_s = 30$ I/s. The magnified bottom frame of this illustration (200-ms interval) emphasizes the slight irregularity of this spontaneous activity, notice different time gaps (a) and (b).

by several factors, including the animal's own ventilatory movements [1, 37], changes in water temperature [44], non-physiological or improper electric environment during experiments *in vitro* [5, 6], and mechanical stimulation [38]. The spontaneous activity (λ_s), as defined in our work, corresponds to the activity measured from a nerve fiber from an intact ampulla *in situ*, from a healthy animal completely submerged in seawater, in resting condition, without strong ventilatory modulations, under stable environmental conditions and without any measurable ambient DC or low-frequency electric fields in the water (see figure 1.3).

1.3.3 Sensory transduction in the Ampullae of Lorenzini

The passive electrical properties of the ampulla and the animal's body turn the environmental electric fields into a voltage difference between the capsule's interior and the pore on the skin of the animal [7, 51]. In addition, the fundamental principles of the cell's electrically-excitable membrane are applied to the apical and basal membrane of the ampullary receptor cells, resulting in organs of exquisite sensitivity [6, 27, 28] (see

chapter 3).

During the process of sensory transduction, the Ampullae of Lorenzini act as electric-signal-to-action-potential-rate converters. The electric signal is the electric potential difference across the sensory epithelium constituted by the electroreceptor cells and supporting cells in the walls of the alveoli. In response to this electric signal, the electroreceptor cells of the sensory epithelium change their basal membrane potential, affecting the rate of continuous release of neurotransmitter vesicles in the synaptic ribbons at the base of the sensory cells [11, 46]. The amount of neurotransmitter released at the synapse gap between the electroreceptor cells and the naked nerve endings determine the membrane potentials propagating to the nerve's first node of Ranvier. After the membrane's threshold potential is reached, the action potentials start their travel at the first node of Ranvier and propagate down the afferent nerve fiber (see figure 1.4).

1.3.4 Information carried in the ampullary nerve cells

For nerve cells associated with sense organs that are silent in the absence of sensory stimulus the propagation of action potentials along the nerve fiber reveals changes in the environmental variables of interest. For nerve cells in sense organs like the Ampullae of Lorenzini, the changing rate of action potentials per second, λ, with respect to the baseline λ_s reveals changes in the environmental variables. Hence, the information sent for processing in the central nervous system is encoded in the time between action potential arrivals. Sensory organs with an spontaneous activity experience either an increase or a decrease of the rate of action potentials per second in response to stimuli, therefore the Ampullae of Lorenzini are able to properly reflect the nature of the electric fields in the ocean, with stimuli that can be positive and negative.

In the Ampulla of Lorenzini, a pore-positive electric stimulus, that is, a stimulus that gives the pore a positive potential with respect to the capsule, will inhibit the nerve activity ($\lambda < \lambda_s$). A pore-negative stimulus, on the other hand, will excite the nerve activity ($\lambda > \lambda_s$). For a low-frequency sinusoidal electric field in the water with an amplitude in the linear range of the receptor organ, the maximum λ coincides with the stimulus strongest pore-negative stimulus and the minimum λ coincides with the strongest pore-positive stimulus (see figure 1.4 d). The λ averaged over a period of this

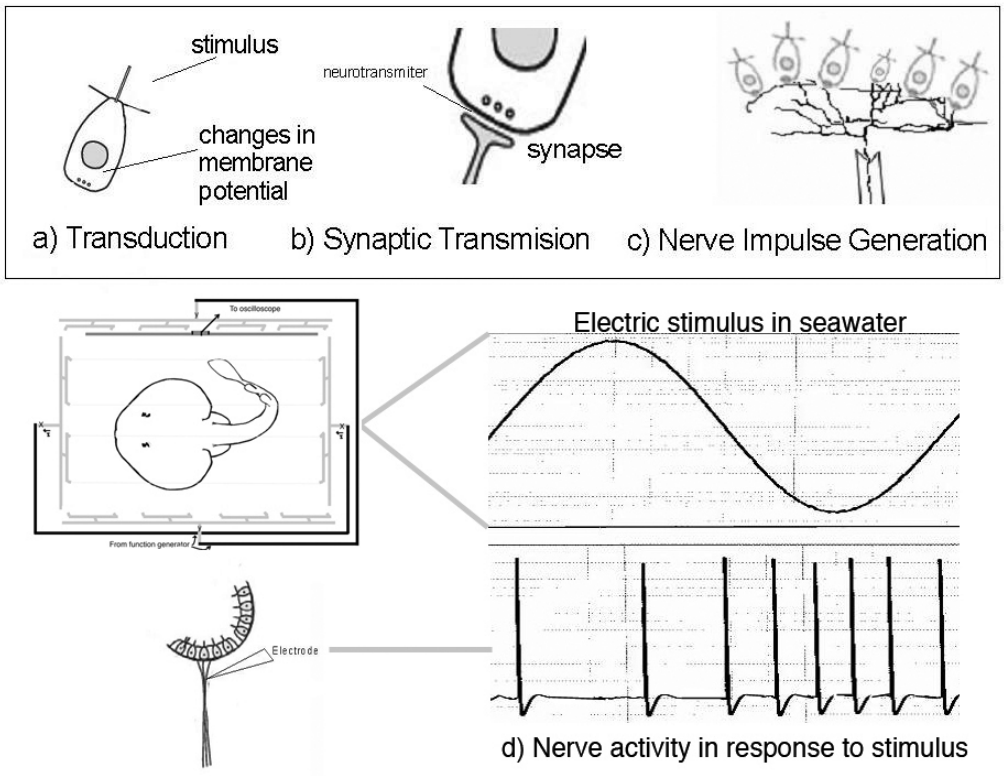

Figure 1.4: Sensory transduction

Schematic diagram of sensory transduction and change in the spontaneous nerve activity of the Thornback ray. a) Transduction: In response to an electric stimulus, the electroreceptor cells of the sensory epithelium change their membrane potential, affecting the synaptic transmission (b). The amount of neurotransmitter released at the synapse determines the generation of action potentials (c) and thereby the rate of action potentials per second (λ) in the afferent nerve fiber. (d) Changes in the spontaneous activity λ_s point to changes in the environmental variables. For a low-frequency sinusoidal electric field in the water with an amplitude in the linear range of the receptor organ, the maximum λ coincides with the strongest pore-negative stimulus and the minimum λ coincides with the strongest pore-positive stimulus.

sinusoidal stimulus should still be λ_s (see chapter 6).

1.4 Electrophysiological recordings

The thornback ray's behavior and anatomy make this animal an ideal subject for electrophysiological studies of the electric sense. The fish's natural tendency to lie flat on the bottom allows performing *in vivo, in situ* nerve fiber recordings while only gently restraining the animal. A miniature suction electrode, gently touching the exposed hyomandibular nerve bundle, records the activity of the nerve fibers without the puncturing typical of glass microelectrodes. This procedure, developed by Dr. Ad. J. Kalmijn at Scripps Institution of Oceanography, allow us to continuously perform recordings on a healthy animal over several days. During my collaboration with Dr. Kalmijn, we added the ability to process and analyze two nerve fibers simultaneously during the experiment, and to generate DC and low-frequency electric fields not only parallel but also perpendicular to the animals' longitudinal body axis (see chapter 4).

1.5 Data analysis and linear dynamic range of response

At the end of each recording of the sensory response to a periodic signal with a particular amplitude and frequency we generate a period histogram of the nerve fiber's activity. The histogram gives the distribution of action potentials during the stimulus period, accumulated over a number of stimulus cycles. The number of cycles for each trial is determined by the total count of action potentials (see chapter 5).

The determination of the ampullary nerve's threshold of sensitivity is done for sinusoidal stimuli as a function of frequency, exploring the response to different amplitudes using 3dB steps. A sense organ with a constant spontaneous activity does not have a threshold of sensitivity determined by the ability of the rate of action potentials to encode the stimulus, but determined by the response of the nerve fiber with respect to the noise of the system. We use non-linear regression to fit a sinusoidal envelope to the data in the period histogram. This sinusoidal function is the response of the nerve to a sinusoidal stimulus, and the noise of the system is represented by the variance in the period histogram. Subsequently, we use analysis of variance to test the significance

of the regression. The threshold of sensitivity recorded for a nerve fiber is defined as the smallest stimulus amplitude that produces a statistically significant regression at the 5% level (see chapter 6). The determination of the maximum stimulus amplitude with a linear response in the nerve fiber is done by visual inspection of the period histogram. It is simply the largest amplitude producing a histogram without clipping of the sinusoidal envelope.

2

DC and Low-Frequency Electromagnetic Fields in the Ocean

2.1 Electrical properties of seawater

The physical properties of seawater determine its electrical conductivity as a function of the frequency of the electric fields involved. For electric fields in the DC or low-frequency AC range, the mobility and concentration of ions dissolved in the water are the factors that determine the conductivity, as their movement constitutes the resulting electric current observed in the water. For high-frequency electric fields and for electromagnetic wave propagation the mechanism of conduction changes, the dielectric properties of the water itself become the main factor in the electric conduction.

If we impose a DC electric field in the seawater by means of a pair of electrodes connected to a battery, we will observe an ionic current passing between the positive electrode (anode) and the negative electrode (cathode). Negative ions (anions) such as chloride, will move towards the anode, and positive ions (cations) such as sodium will move towards the cathode. The combination of those two opposite ionic flows constitute the net electric current in the water. The resulting current density follows Ohm's law: $\overrightarrow{J} = \sigma \overrightarrow{E}$, where σ is the conductivity of seawater and represents the volume charge

density and mobility of the positive and negative charges in the water [47] (see appendix A).

Ohm's law is also expressed as $\overrightarrow{E} = \rho \overrightarrow{J}$, where ρ is the resistivity of the seawater. It is possible to produce an electric field by using a current source with a pair of electrodes attached to opposite walls of a seawater tank. We may then calculate the strength of the electric field in the middle of the tank:

$$E = \rho \, (\frac{Current}{Cross - sectional \ Area}) \tag{2.1}$$

2.2 Ambient electromagnetic fields in the ocean

2.2.1 Induced electric fields

Low frequency electric fields and DC electric fields are common in the ocean. As predicted by Faraday [10], the motion of a body of seawater can be detected by observing the effects of electromagnetic induction; a conductor moving in a magnetic field will experience an electromotive force perpendicular to the velocity of the conductor and the magnetic field, with a magnitude proportional to the product of their strength and the sine of the angle between the two ($\overrightarrow{v} \times \overrightarrow{B}$). This force will induce the movement of the ions in the water, and accumulation of charges in the boundaries of the oceanic current. The resting water around the oceanic current and the seabed complete the electric circuit allowing the continuous passage of electric current. The current density $\overrightarrow{J}$ across the oceanic current is inversely proportional to the resistance across the body of water and the return path (see appendix B).

With the ocean currents flowing mostly parallel to the surface of the earth, and the air above the surface being a poor conductor, the relevant information regarding the drift in surface ocean currents comes from the horizontal electric currents generated by interaction with the vertical component of the magnetic field of the earth [33]. Wind-driven ocean currents are not the only sources of induced electric fields. Tidal flows normally extend to the sea bottom in the coastal waters and channels, generating electric fields highly influenced by the conductivity of the sea bed. In deep ocean currents, a small field is generated by interaction with the magnetic field of the earth.

Table 2.1: Earth-current disturbances under different oceanic conditions, measured at shore. Values in the ocean typically 1/5 of those values. Reference values in mV/Km. From Von Arx [49].

Period	Storm	Disturbed	Quiet	Minimum
Diurnal	>26.5	3.5-11.5	3.0-4.0	3.0-4.0
30-60 min	11.5-26.5	11.5-26.5	1.0-3.5	<1.0
10-30 min	11.5-40	3.5-18.0	1.0-3.5	<1.0
1-10 min	11.5-18	2.0-11.5	1.0-3.5	<1.0
<1 min	3.5-6.0	1.0-2.0	<1.0	<1.0
<1 sec	2.0-6.0	1.0-2.0	<1.0	<1.0
<1 sec	2.0-6.0	1.0-2.0	<1.0	<1.0
	(1 mV/Km =	100 nV/cm)		

2.2.2 Fields of atmospheric and terrestrial origin

The sources of electric fields are not restricted to the ocean. The electric phenomena in the atmosphere and earth's crust introduce extra electric features (see table 2.1). Kalmijn's detailed description of relevant electric features produced by atmospheric, telluric and electrochemical phenomena is available at [20]. For the field strength of selected electrical features in the ocean please see table 2.2.

2.2.3 Complexity of the ambient electric fields

The resulting additional electric fields may generate an electric seascape that is difficult to translate and decompose into simple electric features. On the other hand, the additional complexity introduces more information about the environment. The ability to extract biologically relevant features from this rich electric ocean have contributed to the success of sharks and rays over several geologic periods.

Particular behaviors of the animal are accompanied by the occurrence of some particular electric features. The animal's expectations of the electric fields in the ocean play a significant role in the sensitivity of the sensory system. Sharks and rays have an astonishing ability to sense and orient to extremely weak electric fields, and also to locate local sources in the presence of complex ambient electric fields.

Table 2.2: Magnitude of selected electrical features in the ocean [20, 45]

Electric Field:	Magnitude
Induced Fields	
Wind driven ocean currents N. Atlantic	50 to 500 nV/cm (Von Arx)
Tidal Stream in the English Channel	250 nV/cm (Longuet-Higgins)
Diff. between flood and ebb peek flow in salt march	660 nV/cm (Sanford)
Fields due to Geomagnetic variations (<5 Hz)	
Telluric daily var. in coastal and continental shelf	50 nV/cm (Cox)
Currents induced by magnetic storms (Earth)	10-1000 nV/cm
Micropulsations (Earth)	10-5000 nV/cm
Electric anomalies 1- 8 hours before earthquakes	500 nV/cm (Fedotov)

2.3 Electric fields of biological origin

The bioelectric fields in the ocean are of high biological relevance for sharks and rays. During the process of evolution, elasmobranch's have learned to recognize the weak bioelectric fields generated inadvertently by prey or enemies in the ocean, and to locate their source. Electric fields simulating prey in the water are sufficient to elicit robust feeding responses, showing that sharks and rays in their final attack heavily rely on their electric sense.

Kalmijn's initial endeavor to measure the bioelectric fields generated by different individuals representing 60 seawater species still constitutes the most comprehensive data available [18]. The measurements did not focus on a description of the rather complicated and variable configuration of the bioelectric fields, but on giving an idea of the strength of the field 1 mm away from the skin, the location of hot spots in the body, the modulations of the field due to animal's movement, and the effect of skin injuries on increasing the field strengths. The bioelectric fields of sharks and rays are significantly smaller than the fields of the other fishes in the study (see table 2.3).

Table 2.3: Bioelectric potentials in the water 1 mm from the body surface of marine animals, referred to a remote electrode. From Kalmijn [20]

Material Systematic position	no. of species	max. DC normal μV	max. DC wounded μV
CHORDATA			
Osteichthyes	6	500	> 500
Chondrichthyes	2	50	> 50
Tunicata	4	100	-
ECHINODERMATA	17	10-80	$\sim$
ARTHROPODA			
Crustacea	4	50	1250
MOLLUSCA			
Gastropoda	4	100	$\sim$
Lamellibranchiata	3	10	$>$
Cephalopoda	2	1	$>$
ANNELIDA	4	10	$\sim$
SIPUNCULOIDEA	1	10	$\sim$
ECHIUROIDEA	1	10	$\sim$
COELENTERATA	9	10	$\sim$
PORIFERA	3	1	$\sim$
-insignificant or not explicitly measured	>somewhat higher	$\sim$about the same	

2.3.1 The mathematical representation of a bioelectric field

One of the main features of the bioelectric field of aquatic animals is the animal's DC electric field. That feature by itself is sufficient to elicit feeding attacks when presented to foraging elasmobranch fishes.

Mathematically, an arbitrary DC electric field can be expressed as a multipole series expansion. Decomposing the total field as the sum of a monopole, a dipole, a quadrupole, and higher terms represents all the possible DC features of the field. For live animals in the ocean, the bioelectric fields can not have a monopole component, because animals are not only sources, or only sinks of ions, but they are both, constantly interchanging ions with the seawater. The continuity of the electric current in the seawater requires it to have a constant flux of ions going out, and into the fish. Hence, the lowest order moment that represents the animal's bioelectric field is the dipole.

The different electric moments fall of exponentially with distance, with the higher order moments falling off more rapidly. Therefore, for a distance far enough from the animal the complexities of the field have faded off, and only the dipole component of the prey's field remains.

The electric field for a point $\overrightarrow{x}$ due to a dipole $\overrightarrow{p}$ at a point $\overrightarrow{x_0}$ is described by the equation:

$$\overrightarrow{E}(\overrightarrow{x}) = \frac{1}{4\pi\varepsilon_0}\left(\frac{3\overrightarrow{n}(\overrightarrow{p}\cdot\overrightarrow{n}) - \overrightarrow{p}}{|\overrightarrow{x} - \overrightarrow{x_0}|^3}\right) \tag{2.2}$$

Where $\overrightarrow{n}$ is a unit vector directed from $\overrightarrow{x_0}$ to $\overrightarrow{x}$ [16].

A dipole $\overrightarrow{p}$ along the z axis, produces an electric field of the form:

$$\overrightarrow{E}(r,\theta,\phi) = \frac{1}{4\pi\varepsilon_0}\left(\frac{2p\cos\theta}{r^3}, \frac{p\sin\theta}{r^3}, 0\right) \tag{2.3}$$

For a dipole generated by a current I with the source and sink separated a distance d in seawater of resistivity ρ, the field components are:

$$\begin{aligned} E_r &= \frac{\rho}{2\pi}\left(\frac{Id\cos\theta}{r^3}\right) \\ E_\theta &= \frac{\rho}{4\pi}\left(\frac{Id\sin\theta}{r^3}\right) \end{aligned} \tag{2.4}$$

Where r ($r \gg d$) is the distance from the dipole and θ is the angle with respect to the dipole axis.

The validity of using a dipole to represent the main field given off by a prey in the water was established experimentally by the feeding response of sharks and rays to electric dipoles in the laboratory and at sea [19, 24].

Prey resting on the seafloor is adequately described as a horizontal dipole in a conducting half-space [3, 50]. In an ideal case, the seafloor reduces the loading of the dipole to half of the loading of an infinite ocean, thus the conducting half-space electric field strength is twice the full-space electric field: $\tilde{E} = 2E$ [32].

The field along the dipole axis for prey resting on the seafloor [24] is then:

$$\tilde{E}_{(\theta=0)} = \frac{\rho I d}{\pi r^3} \tag{2.5}$$

We may then calculate the electric field strength along the dipole axis at different distances from the source. For prey with dipole momentum $p = 40\ \mu Acm$ in seawater with $\rho = 23\Omega cm$ the field strength at different distances from the source are:

Distance from the source	Electric Field Strength
8.4 cm	500 nV/cm
18 cm	50 nV/cm
38 cm	5 nV/cm

At sufficient distance from their bioelectric fields, aquatic animals appear mainly as dipoles. When the predator gets closer to the prey the higher electric moments will be more dominant, and when it is close enough, the different sources and sinks of electric current, or hot spots, dominate the electric field configuration.

2.4 The swimming animal's induced electric fields

For sharks and rays moving in the earth's magnetic field, the electromotive force acting on them is nothing but an electric field $-\rho\overrightarrow{J}$. Hence, their electric sense gives them the ability to orient in the magnetic field of the earth.

The description of the induced electric field experienced by a swimming animal is similar to the induced electric field described for electric fields of ocean currents. When the animal moves in the magnetic field of the earth, it generates an electromotive force in its body that is perpendicular to the velocity of the animal and the magnetic field, with a magnitude proportional to the product of their strength and the sine of the angle between the two ($\overrightarrow{v} \times \overrightarrow{B}$) (see appendix B).

The seawater around elasmobranch fishes has very low resistivity compared to the body of the animal, hence, there is a near-maximal electric current density $\overrightarrow{J}$ flowing across the animal and back trough the seawater. The electric field $-\rho\overrightarrow{J}$ is then almost equal to $\overrightarrow{v}\times\overrightarrow{B}$ in the body tissue ($\overrightarrow{v}\times\overrightarrow{B}-\rho\overrightarrow{J}_{body} \approx 0$). On the other hand, a differential pair of ampullae parallel to $\overrightarrow{v} \times \overrightarrow{B}$, acting as a high-ohmic voltmeter ($-\rho\overrightarrow{J}_{ampulla} \approx 0$), will experience the full extent of the induced field.

An animal swimming in equatorial waters with a speed of 100 cm/s in an easterly direction, in a horizontal magnetic field with a magnetic induction of 40 microteslas, induces a dorsoventral electromotive force $\overrightarrow{v} \times \overrightarrow{B}_h = 400nV/cm$. The animal swimming with the same velocity in more temperate waters induces a $\overrightarrow{v} \times \overrightarrow{B}_h = 100nV/cm$ due to the decreasing horizontal component of the magnetic field of the earth near the poles.

The same fish may induce a right-left $\overrightarrow{v} \times \overrightarrow{B}_v = 600nV/cm$ by interacting with the vertical component of the magnetic field of the earth (up to 60 microteslas in the northern hemisphere) [25]. The right-left induced force in the northern hemisphere of the earth and the left-right induced force in the southern hemisphere are independent from the animal heading. In contrast, the dorsoventral electromotive force gives the animal information about its magnetic heading [21, 22, 25, 29].

3

The Thornback Ray, *Platyrhinoidis triseriata*

3.1 Description and habitat

The thornback rays (*Platyrhinidae*) are represented by two genera and at least three species. Only *Platyrhinoidis triseriata* inhabits California waters.

The head, trunk, and dorsal fins of *Platyrhinoidis triseriata* form a heart-shaped disc wider than it is long. The tail is thin and longer than the disc, and the caudal fin without a distinct lower lobe. The animal gets its common name from three rows of spines on the back and tail. Males mature at 37 cm and females at 48 cm, the maximum recorded size is 91 cm long.

Thornback rays are found inshore, on the mud and sandy bottoms of bays and coastal beaches, and around kelp forests. They feed on worms, crabs, shrimps, squid and small bony fishes [9].

Figure 3.1 is a picture of the dorsal and ventral disc surfaces from a thornback ray. The dorsal surface is light olive to brown and the ventral surface is cream white. Some of the subcutaneous canals and ampullary pores are visible in the picture.

Figure 3.1: Adult male thornback ray, 18 cm disc diameter

Left side of the picture shows a dorsal view of the ray's half disc. The subcutaneous canals of several Ampullae of Lorenzini are visible as lighter lines on the the skin's surface. Right side of the picture shows a ventral view of the thornback ray's half disc. Pore distribution for some ampullae are visible as dark dots on the skin. Some ampullary canals are visible as darker lines on the skin making a fan-like shape. A careful observation on a light table and some dissection under a microscope allow us to separate pores associated with the electric sense from those related to the lateral line sensory system.

3.2 The Ampullae of Lorenzini in *Platyrhinoidis*

3.2.1 Pore distribution

After closely examining two male (disc diameter = 18 cm) and two female (disc diameter = 25 cm) thornback rays, we estimated that near 78% of the total number of ampullary pores are located on the ventral surface of the animal. For the males the estimated total number of pores was 800, and for the females 1,200.

The Ampullae of Lorenzini cluster in four paired capsules. These capsules are distributed with left-right symmetry in the body. According to Montgomery [37], the ampullae count for one half of the thornback ray is 12 from the mandibular capsule, 62 from the supraorbital capsule, 74 from the suborbital capsule and 331 ampullae from the hyoid capsule with pores on the ventral surface. The suborbital and mandibular capsules only group ampullae with pores on the ventral surface. For the dorsal surface, the count is 11 from the supraorbital and 92 ampullae from the hyoid capsule (see figure 3.2). That is, nearly 73% of the ampullae of the thornback ray are grouped in the hyoid capsules.

3.2.2 Canal orientation and length

On the ventral surface of *Platyrhinoidis* the supraorbital ampullae have radial configuration, the suborbital ampullae have a fan-like distribution expanding in the outer buccal area, the small mandibular ampullae follow the contour of the lower lip and the hyoidal ampullae are oriented in many directions [37]. The dorsal surface has supraorbital ampullae mostly oriented parallel to the anteroposterior axis. On the other hand, the hyoidal ampullae have a wider range of orientations, from the hyoidal lateral ampullae showing a fan-like configuration, to the hyoidal medial ampullae, oriented perpendicular to the anteroposterior axis and pointing towards the medial area, to the hyoidal anterior and posterior ampullae, oriented parallel to the anteroposterior axis (see figure 3.3).

The canal orientation, canal length, and skin resistance contribute to the effective stimulus in the Ampullae of Lorenzini. Receptors with short canals rely mostly in the voltage drop across the skin, while longer canals take advantage of the voltage drop across the internal tissue produced by uniform electric fields in the ocean.

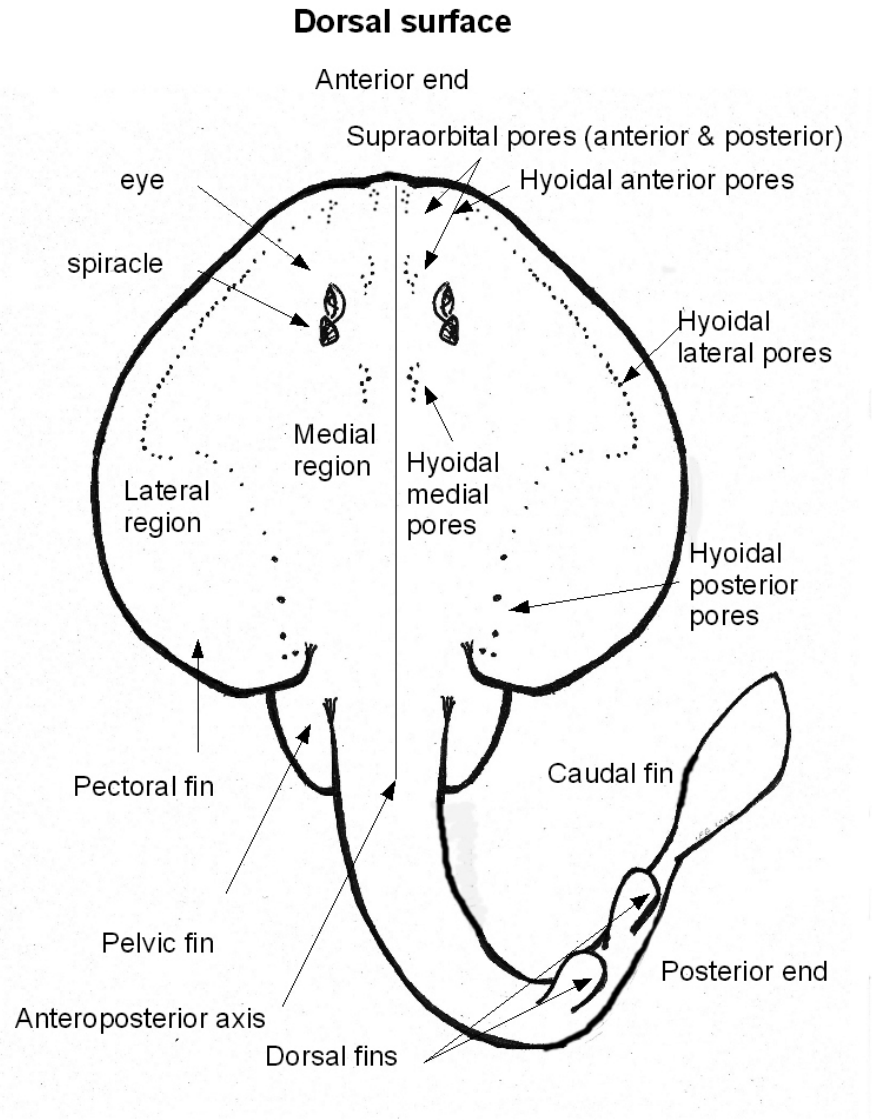

Figure 3.2: Dorsal surface of the thornback ray

Ampullary pores are marked as dark spots on the skin. Nearly 22% of the thornback's ampullary pores are on the dorsal surface. Of those, around 14% belong to the supraorbital and 86% to the hyoid capsules.

Kalmijn [20] measured the potential distribution under the skin of *Platyrhinoidis* submerged in a large volume of seawater ($\rho = 25\Omega cm$). For uniform DC and low-frequency sinusoidal fields perpendicular to the anteroposterior axis, the voltage gradients in the rostral area were about 40% of the voltage gradients in the seawater directly over the skin of the animal. In the pectoral area they were about 55%. For higher frequencies (8Hz) the voltage gradients where respectively 60% and 80% of the voltage gradients directly over the skin of the animal. Hence, the further the ampulla proper can be inside the body, the greater gain in the effective stimulus due to the voltage gradients in the internal tissue of the animal.

For local dipole electric fields at 1 cm from the skin, the internal voltage gradients were less than 5% of the voltages gradients in seawater. Hence, the thornback ray relies in long canals to enhance the effective stimulus in the presence of ambient DC and low-frequency electric fields, but relies mostly in the voltage drop across the skin to detect local electric fields in the close proximity.

3.2.3 Innervation of the ampulla

Under 40X magnification, the Ampulla of Lorenzini seems to have an ampulla proper formed by 4 to 8 alveoli and innervated by a single fiber (figure 3.4 a), higher magnification reveals individual tightly packed nerve fibers innervating the ampulla (figure 3.4 c); up to ten afferent nerve fibers innervate each ampulla transmitting the activity of thousands of electroreceptor cells to the central nervous system of the animal.

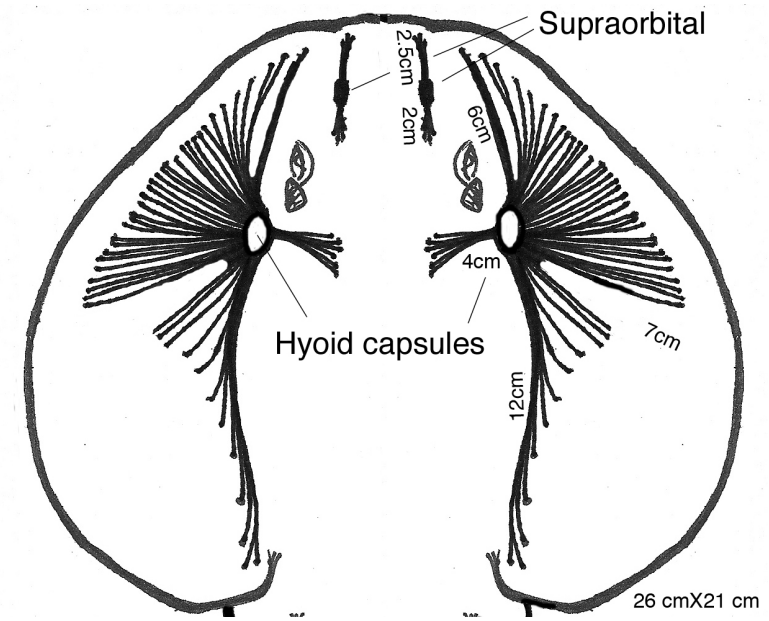

Figure 3.3: Subcutaneous ampullary canals

Diagram of thornback's dorsal surface, showing subcutaneous ampullary canals. Adult female with a 26 cm disc diameter. To group the ampullae proper in capsules allow then to work in common mode. The longer canals run parallel to the anteroposterior axis, giving a total 18 cm of separation between the hyoidal anterior and posterior pores, or a difference of 90 nV between the two pores for an anteroposterior ambient electric field of $5nV/cm$ strength. In contrast, the supraorbital anterior and posterior pores have a maximum separation of 4.5 cm for a difference of only 22.5 nV for the same field.

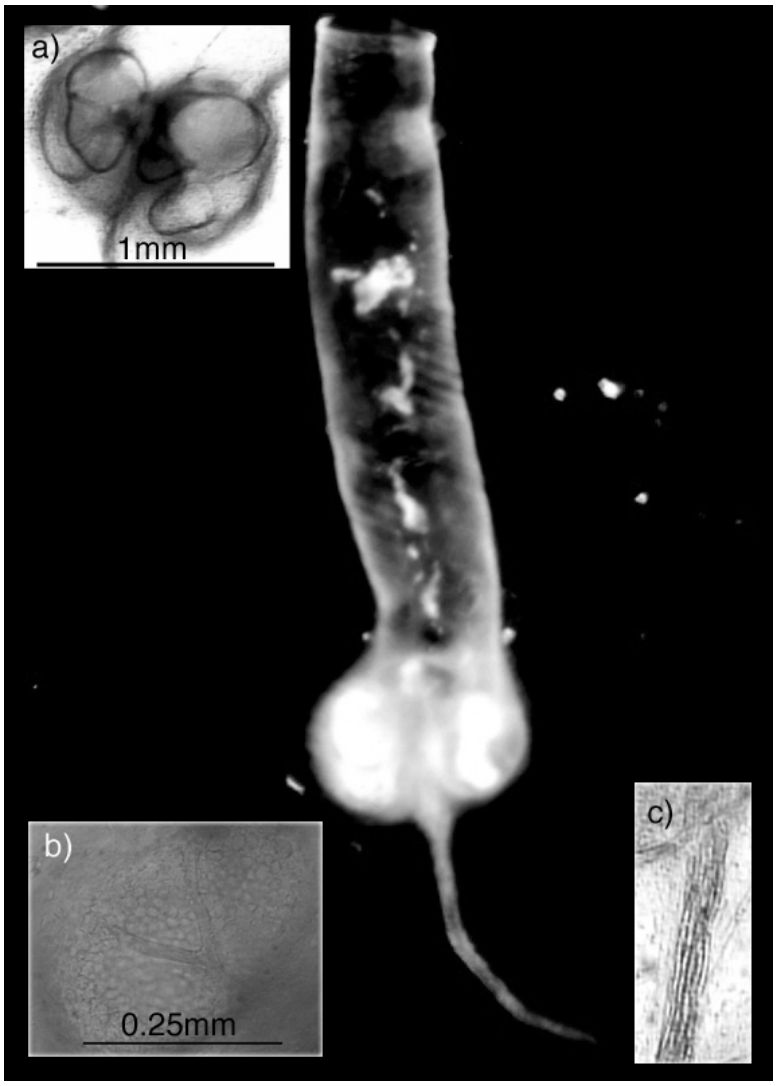

Figure 3.4: Dissected Ampulla of Lorenzini from the thornback ray

Top: short section of the canal. Middle: ampulla proper. Bottom: Ampullary nerve fibers. a) Ampulla proper. b) Alveolus forming the ampulla proper. c) Nerve fibers, Up to ten afferent nerve fibers innervate each ampulla.

4

Data Acquisition

4.1 Increasing the meaningful information obtained from one animal

The original experimental setup at the Sensory Biophysics Laboratory required several years of development and innovation by Dr. Ad. J. Kalmijn. He extended the useful experimental time per animal under the principle of constantly improving the recording's quality and reducing the amount of animals needed for obtaining results. The setup allows us to perform long recordings from live animals kept in the best possible conditions, and increases the amount of meaningful data per hour by providing immediate feedback with real-time statistical analysis of the nerve fiber's activity and organ's response.

4.2 *In vivo, in situ* electrophysiological studies of the ampullae

The goal of the experimental setup is to gain access to the information received by the animal's central nervous system immediately after sensory transduction, by analyzing the electric activity of afferent nerve fibers associated with the Ampullae of Lorenzini.

Other studies available in the literature use excised ampullary organs, placed in

an artificial environment emulating the physiological conditions inside the animal [4,34]. This technique is not necessarily the best for studying the nervous activity of the ampulla; the excised organs are short-lived, and their spontaneous nerve activity is erratic, suggesting a high rate of organ damage. Even without organ damage, poor emulation of the animal's physiological and electrical conditions may result in regenerative responses in the ampulla, devoid of the shunt resistance from the body and seawater [28, 29]. Recording from an intact ampullae *in vivo* increases the duration of the experiments and eliminates those artifacts.

4.3 Electrophysiological experiments in the thornback ray

The ray's tendency to lie flat on the bottom of the ocean for long hours and its peaceful nature make it an ideal subject for electrophysiological studies of the Ampullae of Lorenzini. The dorsal access to the hyomandibular nerve bundle entailing only minor surgery allows us to keep the animal in a natural position while performing experiments. A miniature suction electrode, gently touching the exposed nerve bundle, records the activity of the nerve fibers with minor damage. This gentle procedure allows us to perform *in vivo* recordings from a healthy animal for a week.

4.3.1 Animal handling

All procedures described here are part of the UCSD's Institutional Animal Care and Use Committee protocol number S00257R, reviewed and approved annually during the duration of the experiments. The animals were captured by Ivan F. Gonzalez and volunteer helpers under the Scientific Collecting Permit number SC-008106, renewed annually by the Department of fish and game, State of California.

The rays used for the experiments are caught with hook and line from the Scripps Institution of Oceanography's pier and held in open-circulation seawater tanks at the Electromagnetic Research Facility (EMRF) for weeks.

When the animals display a healthy appetite, they are tested using an electrically-simulated prey ($p = 40\ \mu Acm$) buried under the sand of the tank. If a foraging ray is able to detect the simulated prey and display a characteristic prey-attack behavior, the

animal is declared to be ready for electrophysiological experiments and transported to the electrophysiological room of the Sensory Biophysics Laboratory.

After being transported to the electrophysiological laboratory, the ray is held inside an aerated seawater container to smoothly transition from the seawater temperature at the EMRF to the temperature in our experimental tank. To minimize the temperature difference experienced by the animal, the experimental room is keep only 1℃ or 2℃ below the EMRF's seawater temperature.

After adjusting to room's temperature, the animal is submersed in a solution of 0.5 g of MS222 in 10 L of seawater in a small aerated container. Within approximately 30 minutes of starting the anesthesia, the thornback ray is calm and ready for weighing and injection of relaxant. The animal is injected with 1 ml of Pancuronium bromide solution (0.1 mg/ml of ray ringer) per kilogram of body weight, with half of the dose on each side of the tail. The ray is immediately placed inside the experimental tank, and gently restrained with rubber bands. Two soft rubber hoses are inserted in the spiracles, passing aerated seawater to keep the gills ventilated. The degree of relaxation is checked by soft pinches in the caudal fin of the animal. Pinches producing small movements of the pectoral and pelvic fins indicate an adequate level of relaxation, allowing fast feedback during surgery if the animal is feeling a level of discomfort similar to a tail pinch or bigger. Finally the animal is left overnight to allow some time to adjust to the new environmental conditions, and the thermostat lowered to slowly reach 15℃ (less than 2℃/day).

4.3.2 Surgery

The next morning, we check the anesthesia level, the skin appearance and the ventilatory movements of the spiracle valves. After cleanning the tank the animal is ready for surgery, unless additional relaxant injections are necessary. If the animal is showing strong ventilatory movements or trying to swim away we inject 1/4 of the original Pancuronium dose and wait an hour before starting the surgery.

The surgery starts by pinching a small section of the skin, posterior and slightly lateral to the spiracle, and cutting a small incision as close as possible to the spiracle. From that initial incision it is necessary to remove the skin little by little, moving towards

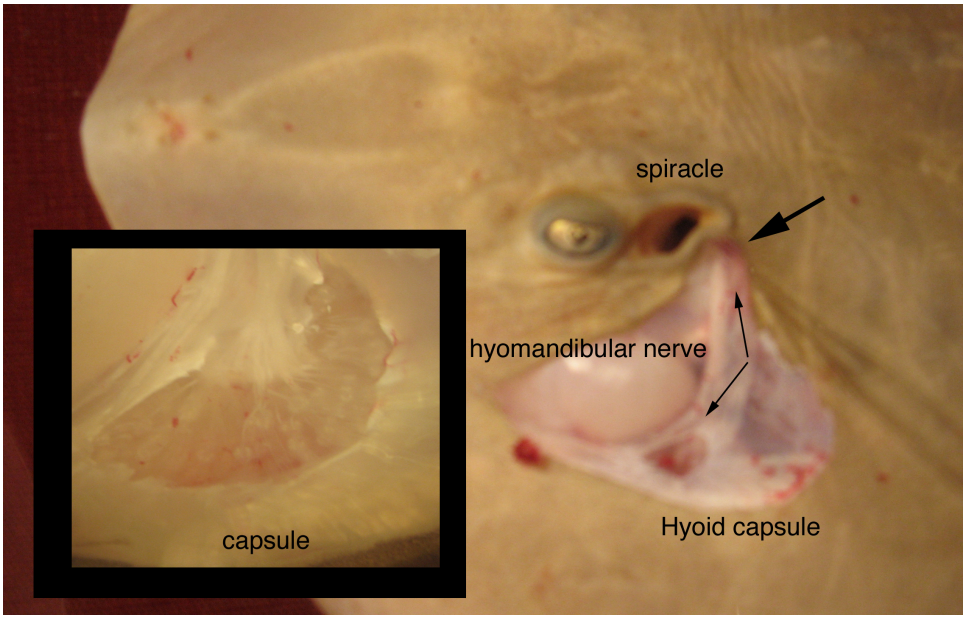

Figure 4.1: Hyomandibular nerve and hyoid capsule

Post-mortem dissection of thornback ray. Actual electrophysiological recordings require only a small incision on the skin area marked by the arrow, expanded to have enough access to the nerve fibers near the cranial area. The open hyoid capsule shows a group of ampullae proper in a grape-like configuration.

the periphery. A subcutaneous tendon marks the most central region of the hyomandibular nerve accessible for surgery, and a set of superficial hyoidal medial canals mark the last point were the nerve bundle runs mostly horizontal before diving into the body to reach the hyoidal capsule. After carefully cutting and removing the tissue covering the nerve fibers, the preparation is ready for electrophysiological recordings. Figure 4.1 shows the full length of the hyomandibular nerve bundle and the hyoid capsule.

4.3.3 Euthanasia

After several days of electrophysiological recordings the animal condition starts to deteriorate. External signs of deterioration are the lack of reaction to tail pinch, sporadic movement of the spiracle's valves, or growth of slime on the skin. Internal signs of deterioration are the decreasing spontaneous activity of the nerve fibers, reduction of the percentage of active fibers, and bursting nerve activity. Additionally, the proportion of recordings from nerve fibers in the lateral line organs increases, up to a point when

only lateral line fibers can be recorded.

When the animal deterioration is evident, we proceed to perform euthanasia by administering an overdose of MS222 and disconnect the ventilatory hoses. After 30 minutes the animal is collected in a labeled plastic bag and properly disposed.

4.4 The nerve-recording system

The nerve-recording system consists of a miniature suction electrode and a reference electrode connected through coaxial cables to a differential low-noise preamplifier (PAR-113) and secured in a semi-flexible holder to a single micromanipulator. The miniature suction electrode is used to measure the nerve fiber activity. The reference electrode follows the movements of the main electrode but it is separated and higher in the water level to avoid touching the ray's skin (see figure 4.2).

The capillary glass micropipette tip in the miniature suction electrode is heat-fused by hand to make a suction surface that will not damage the nerve and a small orifice capable of sucking up individual nerve fibers. Inside the micropipette there is a silver wire that connects with the holder base. The holder connects to tubing allowing control of the suction by means of a calibrated syringe .

The preamplifier is electrically floating with respect to the data-acquisition equipment and grounded to the tank by means of two underwater electrodes. To isolate the preamplifier from the data-acquisition equipment, the preamplifier output is connected to an isolation amplifier (EX4-400 Quad).

The output from the nerve-recording electrode is recorded on digital tape (Biologic DTR 1202) before processing, made audible through an equalizer and speakers and made visible on the oscilloscope screen.

4.5 The stimulus

The electric-stimulus system consist of a function generator (HP3314A), a programmable attenuator/amplifier, a stimulus isolation unit (Isolator-10, Axon Instruments), one DC current source (WPI linear stimulus isolation unit), two pairs of carbon stimulus electrodes, one preamplifier (PAR113) and two silver- silver chloride pellet

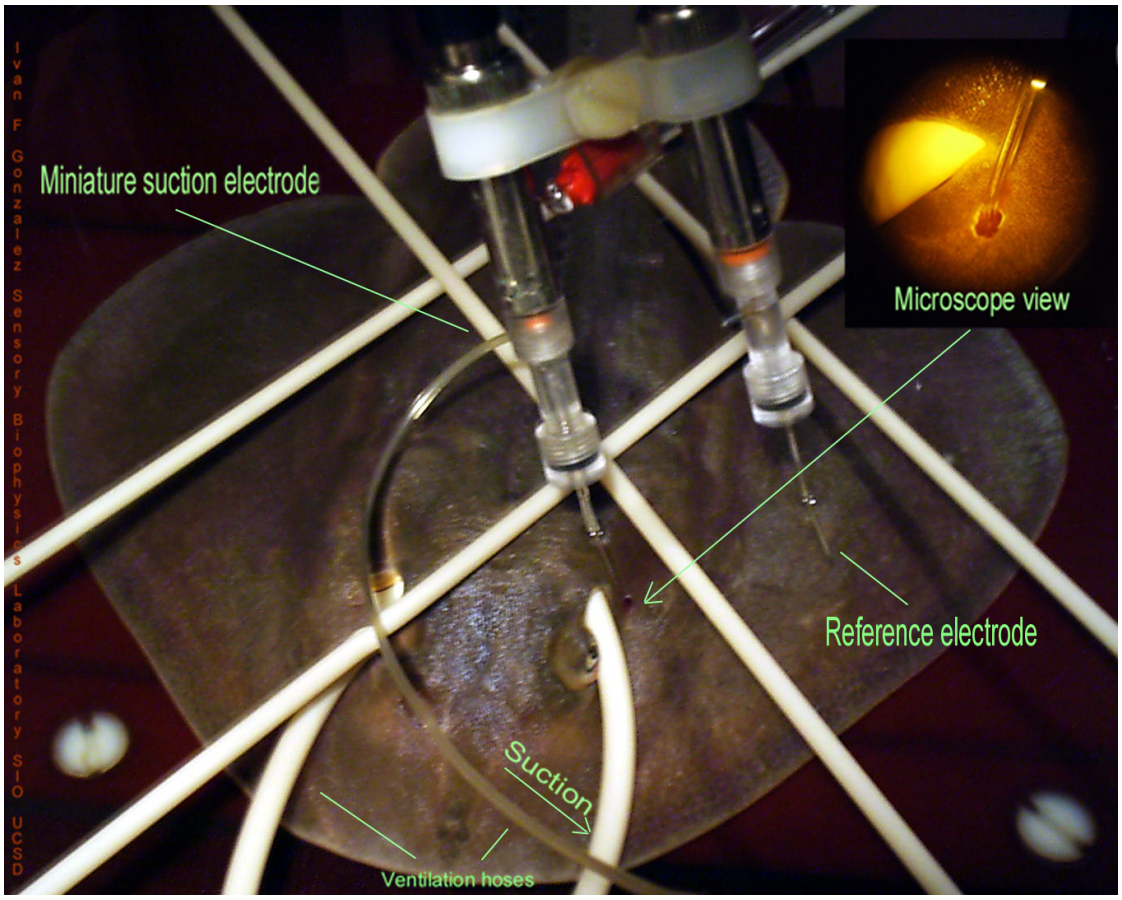

Figure 4.2: Thornback ray inside the experimental tank

Two soft rubber hoses are inserted in the spiracles, passing aerated seawater to keep the gills ventilated. The rubber bands (diagonal) gently keep the animal in place during recording. A small calibrated syringe full of seawater (not shown) controls the suction of the miniature electrode. A small incision on the skin of the animal allows access to the nerve fibers of the hyoidal and mandibular ampullae.

recording electrodes.

The function generator is connected to the stimulus isolation unit. The isolated stimulus goes to a custom-made programmable attenuator/amplifier, and from it to a switch selecting between two perpendicular pairs of salt-bridge diffuser electrodes in opposite walls of the tank. These salt-bridge diffuser electrodes consist of a pair of carbon electrodes inside an inverted T-shaped PVC pipe located at opposite sides inside the tank, partially submerged in seawater. The T-shape pipe splits in symmetrical branches, evenly splitting the stimulus current in symmetrical outputs at the end of the diffuser. The diffusers end in four outputs for the shorter walls, and eight outputs for the longer walls (see figure 4.3).

Two silver- silver chloride pellet electrodes using 35 cm long silicon tubing salt-bridges are positioned at opposite sides of the tank to measure the stimulus in the seawater. The electrodes are connected to a PAR113 preamplifier, and through the programmable attenuator/amplifier, to an isolation amplifier (EX4-400 Quad) and the data-acquisition system.

The programmable attenuator/amplifier has two main purposes; the first is to keep the function generator operating in a range strong enough to have the cleanest stimulus possible even if it means attenuating the output of the function generator for weak stimulus. The second purpose is to keep track of the stimulus in the tank over a wide range of stimulus amplitudes without the need to manually change the recording settings. The stimulus-recording preamplifier is connected to the programmable attenuator/amplifier second input. The microprocessor controller automatically sets the unit to output a scaled signal; therefore, the quality of the stimulus in the tank can be recorded and displayed on the data-acquisition oscilloscope without the need of changing the display settings.

The output from the recording electrodes and the attenuator settings are recorded on digital tape (Biologic DTR 1202). It is important to mention that the function generator is also controlled by the microprocessor; therefore, all of the electric-stimulus system can be automated during recordings.

The integrity of the electric isolation in the seawater tank is maintained by; 1) having the Isolator-10 connected between the function generator and the programmable

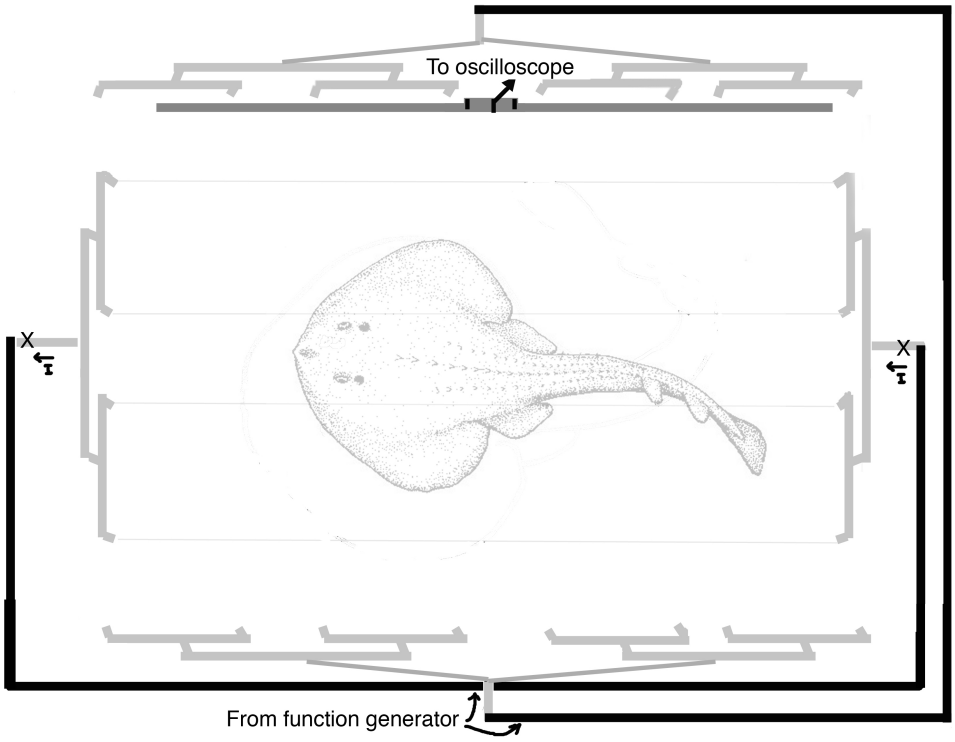

Figure 4.3: Stimulus system

System consisting of two pairs of stimulus electrodes and a pair of recording electrodes, allowing horizontal stimulation in two directions. Additionally to the low-frequency stimulus coming from the function generator, we include a DC current source in the setup when a uniform DC electric field is required.

attenuator, 2) having the output of the seawater recording electrodes differentially entering the data-acquisition system in the EX4-400 Quad amplifier, and 3) using high isolation voltage photocoupler transistors inside the programmable attenuator box to isolate the unit from the microprocessor.

4.6 Exploration of the nerve fiber

After surgically cleaning the access to the nerve, we explore the nerve bundle by gently placing the miniature suction electrode in contact with an area of exposed nerve fibers. During the exploration of the nerve, the manipulation of the miniature electrode is done under a dissection microscope. The signal from electrode is made audible on a set of speakers so the audible clues give most of the information about the nerve recordings while observing under the microscope. A characteristic pop follows a successful suction of the nerve bundle, and the a trace showing several active fibers should appear immediately on the oscilloscope screen (see figure 4.4).

Small position adjustments of the miniature electrode and different suction levels will make one or two of the action potential trains rise above the others and increase the volume of a low-frequency tapping sound, indicating that the miniature electrode has sucked a node of Ranvier of one active nerve fiber. This method of exploring the hyomandibular nerve is biased to only find ampullary fibers that have spontaneous activity.

The nerve fibers from the lateral line system also make up part of the hyomandibular nerve bundle. The lateral line fibers are recognizable for having an irregular rate of spontaneous activity and to respond to water motions. To discard lateral line fibers we test the response to mechanical stimulus (a jet of water or tapping on the table), and also stimulate the ray electrically. If there is a response to mechanical stimulus the fiber is released and we proceed to find another fiber.

If the activity of the fiber changes in response to an electrical stimulus in the tank, then we proceed to try to locate the pore of the ampulla associated with the nerve fiber. For that purpose we use a probe with the source of electric current on the tip and the sink elsewhere in the seawater. When the tip is closer to the ampulla's pore the

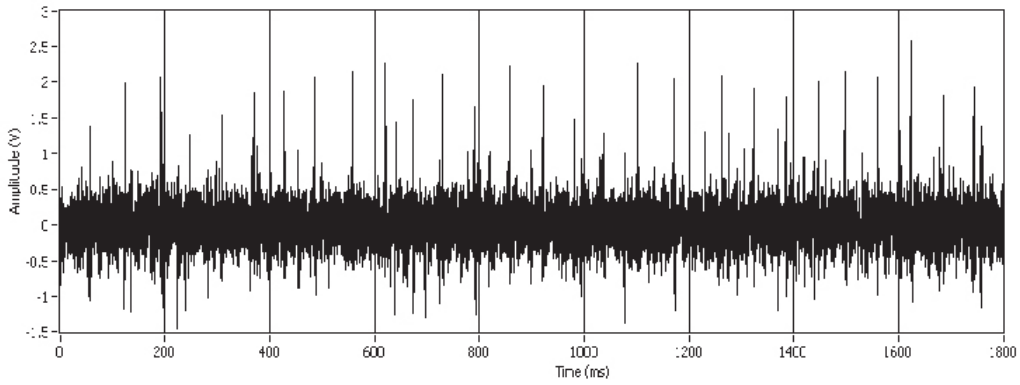

Figure 4.4: Spontaneous activity of the hyoidal nerve bundle after initial suction

The art of manipulating the electrode position and level of suction is to bring one of the nerve fibers with a exposed node of Ranvier close to the tip of the silver wire inside the miniature electrode. The increased relative amplitude of the action potentials from the node of Ranvier of the nerve fiber make them electronically separable from the background activity.

nerve activity changes drastically. This technique is limited to the pores on the dorsal surface of the animal, hence, only one on four of the hyoidal pores can be identified by this method.

5

Data Processing

5.1 Computer interface for data acquisition and real-time analysis

The data processing setup has three main parts: 1) stimulus selection, 2) recording setup and digitalization, and 3) real-time analysis of the response. The experiment is handled by two interlaced microprocessors, one primarily manipulates the experimental conditions and the stimuli, and the other performs the real-time statistical analysis.

The signal received from the miniature suction electrode is displayed on an oscilloscope, played on speakers, stored in a DAT recorder, digitalized, and analyzed. The experimental log and real-time data analysis are displayed on computer screens, printed on a plotter, and saved in computer text files.

5.2 Stimulus selection

5.2.1 Stimulus matrix

Stimulus selection is performed in the "matrix" microprocessor, so named for the grid of different frequencies and amplitudes presented to the user both as a selecting tool and an experimental log, keeping track visually of previous stimulus selections and results. Available wave forms are: square wave, sinusoidal, zero amplitude and pre-programmed arbitrary shape. The lowest frequency available is 0.125 Hz, which can

be increased by factors of $\sqrt{2}$, up to 256 Hz, though frequencies higher than 16 Hz are rarely employed. The matrix central row has a reference amplitude value of 640 nV/cm, with selection steps of 3 dB. The maximum available stimulus amplitude is 57 dB but we rarely use more than 24 dB, as those amplitudes are out of the linear range of most fibers. The minimum amplitude verifiable by direct measurement of the electric field in the seawater tank is -30 dB, and amplitudes less than -36 dB are seldom used as the threshold of sensitivity for most fibers is higher.

5.2.2 Duration of the stimulus

Stimulus duration is not set for a pre-determined time, but rather lasts until a pre-determined total number of action potentials have been observed. The duration of the stimulus then depends on the selected number of action potentials and the activity of the nerve fiber ($t = action\ potentials/\lambda$).

Two additional factors affect the total duration of the stimulus. The first is the requirement that the amplitude of the stimulus be brought up slowly, to avoid transient reactions of the ampulla and capture only the organ's steady state response. The second is imposed by the period histogram analysis. Period histograms require recordings to be performed during an integer number of stimulus cycles, so the recording in the last cycle is not incomplete and the histogram is not biased. Hence, the microprocessor starts the stimulus early to allow the stimulus to reach full amplitude, and subsequently starts counting action potentials, stopping the recording at the end of the appropriate stimulus cycle.

For low frequencies ($f < 1\ Hz$), the variability in the total number of action potentials introduced by the completion of the last stimulus cycle ($\pm\lambda_s/2f$) may become a biasing factor by itself when comparing recordings with low numbers of action potentials. The rule of thumb to avoid this problem is to require at least $10\lambda_s/f$ action potentials per recording, keeping the variability in the number of action potentials under 5%.

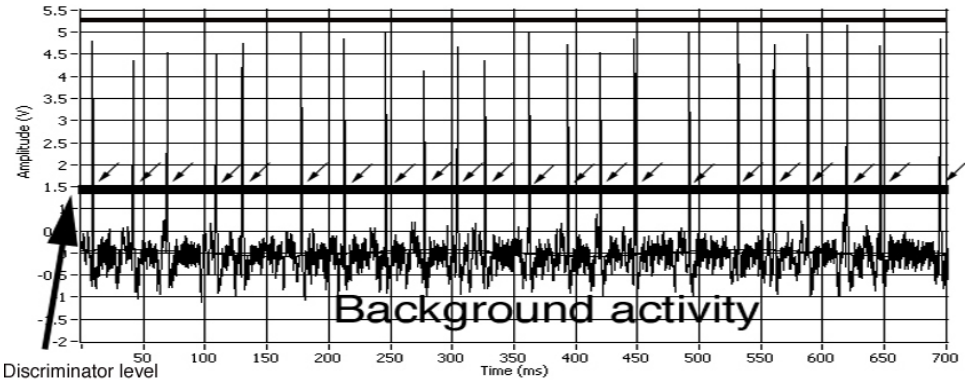

Figure 5.1: Digitalization of the action potentials

Two voltage levels set a window for signal discrimination, with bottom level higher than the background activity and top level higher than the tallest action potential of interest. The window discriminator produces a pulse anytime the action potential reaches the window's bottom on its way down.

5.3 Digitalization of the action potentials

The miniature electrode often suctions more than one nerve fiber. The traditional procedure when activity from more than one nerve is visible on the recording is to release the nerve bundle and suction in another area or to carefully move the electrode to allow the repositioning of the nerve fibers inside the electrode. When one exposed node of Ranvier comes closer to the tip of the silver wire inside the miniature electrode the increased relative amplitude of its action potentials make them separable from the background activity.

A window discriminator (WPI model 121) digitalizes the signal from the miniature suction electrode. With two voltage levels set according to the amplitudes of the action potentials and the background activity, the window discriminator produces a pulse anytime the action potential's amplitude reaches the lower voltage level on its way down (see figure 5.1). The pulses are counted with an HP 5316A counter and directly fed to the real-time analysis microprocessor and the matrix microprocessor. The counter display is of great help even when not recording, displaying the rate of spontaneous nerve activity every second.

Traditional window discriminators are designed for single-unit recordings, unable to sort two different action potential trains. When the recordings show simultane-

ously more than a single action potential train above the background activity, the user had been forced to move the electrode in an attempt to loose one signal, with the hope only one node of Ranvier remains near the tip of silver wire inside the electrode. By contrast, we modified the setup to be able to record and analyze in real time two action potentials trains from the same electrode simultaneously.

5.3.1 Simultaneous recording of the nerve activity from two nerve fibers

The experimental setup is not limited to single-unit recordings from one electrode. We do not discard, but rather take advantage of the cases when signals from two nerve fibers are sufficiently above the background activity and their amplitude is distinct enough to be separated electronically. In that case, one miniature suction electrode carries simultaneously two action potential trains, either the nerve activity of two ampullae, or the nerve activity of two afferent nerve fibers from the same ampulla.

The difficulty of two-unit recording analysis is to sort which action potential belongs to one fiber and which to the other. Even when one unit has an amplitude big enough to be separated from the other by traditional window discriminator techniques, the overlapping impulses have highly-variable amplitudes and the coinciding pulses add to create one giant action potential, making window discrimination unreliable (see figure 5.2). The study of those cases and necessary development of new hardware took advantage of the ampullary simulator to simulate a two-unit action potential train under controlled overlapping and coincidence scenarios (see appendix C and D).

The custom-made action potential sorter takes advantage of recordings where only two action potential trains are above background noise. It detects the overlapping of two action potentials using a time window just shorter than a refractory period in a single nerve fiber. This window is triggered every time a first impulse is received and looks for impulse arrivals during that time window to determine overlapping impulses. The coinciding impulses are detected by setting a high threshold level at a window discriminator, higher than the regular highest amplitude of the high-amplitude action potential train. The output of both detections are compared using a custom-made analog-digital circuit and mixed with the output of two window discriminators. The circuit simply

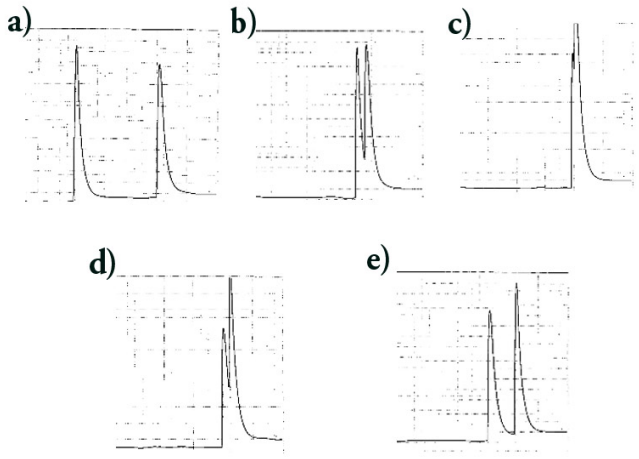

Figure 5.2: Simulation of a two-unit recording

a) and e) show a situation where traditional window discriminator techniques can sort the two units correctly. b) and d) show a situation where traditional techniques fail to sort the two units due to overlapping of the impulses. c) shows a coincidence where there is only one discernible action potential, with amplitude out of the scale.

adds the missing (miscount) pulses to the regular trains separated by traditional window discriminator techniques (see appendix D). The sorted action potential trains are sent as two separated trains of pulses to two real time microprocessors. A switch allows to use either the lower- or higher-amplitude action potential train to feed the counter and matrix microprocessor.

5.4 Real-time analysis

The real-time microprocessors receive a train of pulses for the total duration of the recording and a trigger pulse at the start of every stimulus cycle. To produce a period histogram the computer uses 32 running bins, each with width 1/32 of the stimulus period (with the last bin width adjusted for precise timing). Every time a pulse arrives to the computer, the respective bin count increases by one. Hence, for bins in the excitatory part of the stimulus the pulse count should be high, while bins in the inhibitory part of the stimulus should have low pulse counts.

The results are displayed on the real-time computer screens few seconds af-

ter the stimulus has stopped, giving immediate feedback of the nerve's response to a particular stimulus in the form of a period histogram (see chapter 6).

The real-time screen also displays the measured frequency of the stimulus, stimulus amplitude, number of action potentials, number of stimulus cycles, and λ_s, and generates a unique label for storing the results with a time stamp.

5.4.1 Determination of the nerve's threshold of sensitivity

The determination of the nerve's threshold of sensitivity is done for sinusoidal stimuli at all selected frequencies, one at a time. The results of the statistical analysis are displayed on the real-time microprocessor's screen, with two criteria available for the user:

1) After fitting the amplitude and phase of a sinusoidal envelope to the 32 bins of the histogram using non-linear regression, we use analysis of variance to test the significance of the regression (see chapter 6). The threshold of sensitivity is the smallest stimulus amplitude that produces a statistically significant regression at the 5% level ($P(F_{2,29} > 3.33) = 0.05$).

2) Assuming that the phase of the response is known (preserved from the response to an earlier, higher amplitude reference stimulus), and fitting the amplitude of a sinusoidal envelope to the 32 bins of the histogram using curvilinear regression, we use analysis of variance to test the significance of the regression (see chapter 6). The threshold of sensitivity is the smallest stimulus amplitude that produces a statistically significant regression at the 5% level ($P(F_{1,30} > 4.17) = 0.05$).

In the case that criteria 1) and 2) are not significant at the same time, we repeat the test two more times with the same stimulus, if two of three trials are still significant for the two criteria, we move on to test the next amplitude in the same way.

6

Data Analysis

The data analysis of the electrophysiological data is done in the real-time microprocessors. The results are displayed on the real-time computer screens few seconds after the stimulus has stopped, giving immediate feedback of the nerve's response to a particular stimulus in the form of a period histogram.

6.1 Period histograms

Period histograms are well suited for the analysis of sensory response to periodic signals. The histogram is an estimator of the probability of instantaneous firing of action potentials during stimulus. The histogram is constructed by splitting the stimulus period (T) in N smaller time intervals or bins, and counting the number of action potentials occurring during the respective time interval in a stimulus cycle. The excitatory part of the stimulus has bins with high action potential counts, while the inhibitory part of the stimulus has bins with low counts of action potentials (see figure 6.1).

Repetition of the same stimulus over several cycles generates period histograms where the individual variability of each trial is reduced, generating a smoother estimator of the probability of instantaneous firing rate during stimulus.

The number of action potentials in a bin (y_i), reflects the rate of action potentials per second for that bin (λ_i), averaged over several cycles:

$$\lambda_i = y_i \times (\frac{N}{T \ \times \ number \ of \ cycles})$$

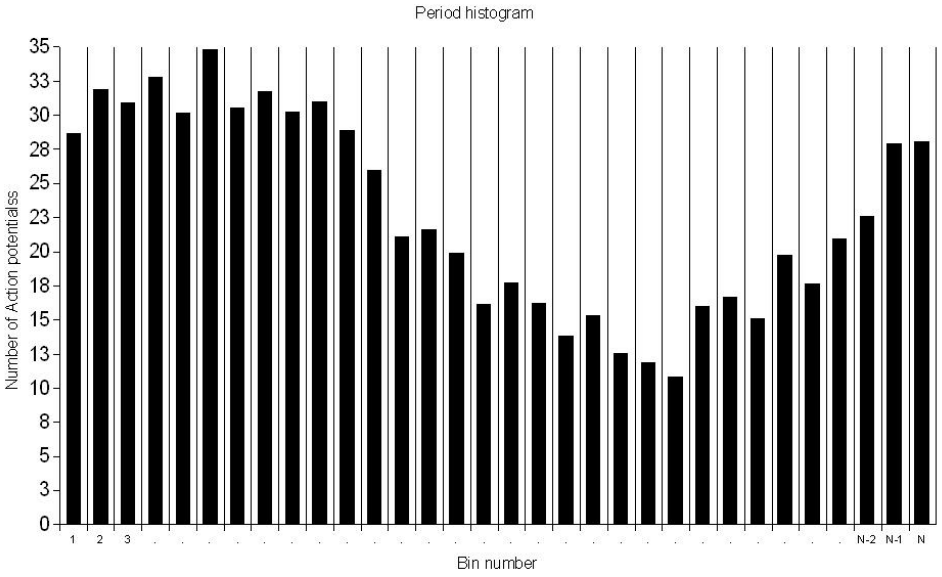

Figure 6.1: Period histogram of sensory response to sinusoidal stimulus

N = number of bins in a period. y_i = number of action potentials in the bin i. The histogram is collected over several cycles, each bin width representing a fraction of the stimulus period.

The bin number i ($i = 1, \ldots, N$) represents the time $t_i = \frac{T}{N}(i - 0.5)$ after the onset of the stimulus cycle, or conversely the stimulus phase $x_i = \frac{2\pi}{N}(i - 0.5)$ where λ_i is measured.

6.2 Statistical analysis of the response to sinusoidal stimulus

The statistical analysis of the period histogram determines the probability that the recorded nerve activity is a result of the stimulus, rather than a natural fluctuation in the spontaneous activity of the nerve.

There is a distinction between the statistical analysis performed for the experiments and the way the animals process information encoded in the action potential trains. The statistical methods determine if the information is available for the animal, but do not attempt to explain the decoding mechanism of the animal.

6.2.1 Computing the histogram's envelope for sinusoidal stimulus

We use the least squares method to find the coefficients of a non-linear regression fit for a sinusoidal envelope of the data in the period histogram in response to a sinusoidal stimulus. To fully characterize the response of the nerve to the sinusoidal stimulus, we fit the function $Y(x) = b_0 + b_1 \sin(x + b_2)$ to the histogram.

$$\begin{aligned} Y_i &= b_0 + b_1 \sin(x_i + b_2) \\ x_i &= \frac{2\pi}{N} i \end{aligned} \tag{6.1}$$

The parameters $b_0,\ b_1\ ,\ b_2$ are found analytically (see appendix F):

$$b_0 = \bar{y}_i \tag{6.2}$$

$$b_1 = \frac{2}{N \cos b_2} \sum_{i=1}^{N} \tilde{y}_i \sin x_i \tag{6.3}$$

$$b_2 = \arctan\left(\frac{\sum_{i=1}^{N} \tilde{y}_i \cos x_i}{\sum_{i=1}^{N} \tilde{y}_i \sin x_i}\right) \tag{6.4}$$

with $\tilde{y}_i \ = \ y_i - \bar{y}_i$.

6.2.2 Analysis of variance

After fitting the level (b_0), amplitude (b_1) and phase (b_2) of the sinusoidal envelope to the N bins of the histogram, we use analysis of variance to test the significance of the regression (see appendix F). We can decompose the total sample variance, t_l, as the part accounted for by the model, R_g or regression mean square, and that which is not, R_s or the residual sum of squares. Because the number of cycles averaged in the period histogram determine the variance of the system, the results of the analysis of variance for different nerve responses are only comparable to responses averaged over the same number of stimulus periods.

$$t_l = R_s + R_g$$

For the least squares fit:

$$\sum_{i=1}^{N} (y_i - \bar{y}_i)^2 = \sum_{i=1}^{N} (Y_i - \bar{y}_i)^2 + \sum_{i=1}^{N} (y_i - Y_i)^2$$

$$t_l = \sum_{i=1}^{N} (\widetilde{y}_i)^2 \tag{6.5}$$

$$R_g = (N/2)^3 b_1^2 \tag{6.6}$$

$$R_s = t_l - R_g \tag{6.7}$$

We perform an F-test which is discussed in more detail in appendix F. To test the significance of the regression we compute $F_{\nu-1,N-\nu}$, where $\nu = 3$ and $N = 32$ are the degrees of freedom for the regression and the histogram respectively.

$$F_{2,29} = \frac{R_g/2}{R_s/29} \tag{6.8}$$

We evaluate how well the histogram is fit by the sinusoid, determining that the sinusoidal response is due to the sinusoidal stimulus for statistically significant regressions at the 5% level ($P(F_{2,29} > 3.33) = 0.05$). We can further refine the significance test by assuming that the phase of the response is known and there is one less degree of freedom in the regression:

$$F_{1,30} = \frac{R_g/1}{R_s/30} \tag{6.9}$$

The histogram is fit by the sinusoid at the upper 5% of the F-distribution when $F_{1,30} > 4.17$.

7

Results

7.1 Results summary

We measure the organ's nerve activity in response to step functions of electric fields, to low-frequency sinusoidal electric stimuli in the presence of various DC fields and to low-frequency sinusoidal electric stimuli of different relative orientation. The Ampulla of Lorenzini of a resting thornback ray has a response that fades out with a time constant of a few seconds after the onset of a constant electric field. Hence, the ampulla effectively adapts to DC ambient electric fields. The Ampulla of Lorenzini shifts its linear dynamic range by adapting to ambient constant fields, allowing sensitivity to small varying electric fields in the presence of strong constant fields. Due to the directional response of the organ, the ampulla presents different linear dynamic ranges of response for sinusoidal electric fields of equal strength but different orientation respect to the animal. The DC adaptation and directional response of the ampullae allow the animal to modulate the electric fields it senses during swimming, effectively widening the linear dynamic range of the electric sense.

7.2 Adaptation to DC stimulus in a resting *Platyrhinoidis*

We studied the adaptation of the ampullary organs in the context of their function for extending the linear dynamic range of the organ. The first results are the characterization of the organ's adaptation response after the onset of constant electric

fields in the water; the second results show the effects of adaptation to constant ambient fields as a physiological mechanism allowing detection of small varying fields in the presence of strong ambient fields.

7.2.1 Response to low-frequency square waves

The responses to square-wave electric stimuli in electrophysiological recordings of the hyomandibular nerve fibers provide an insight into the properties of the Ampulla of Lorenzini and its adaptation to constant fields in the ocean. We explored the characteristics of the organ's DC adaptation by analyzing the responses to 0.125-Hz square waves ($T = 8$ seconds). The amplitude of the stimulus was at the top of the linear dynamic range for each respective nerve fiber, to ensure a high maximum rate of action potentials per second during excitation. Among twenty two realizations in three different animals, eight had an excitatory response ($\lambda/\lambda_s > 1$) following the onset of the stimulus in the water but with λ rapidly returning to λ_s under constant stimulus, ten had an inhibitory response ($\lambda/\lambda_s < 1$) following the onset of the stimulus in the water but with λ also returning to λ_s. The change of stimulus polarity inverted the responses of those nerve fibers. Four realizations had an uncommon response with excitatory responses for both stimulus polarities (see figure 7.1).

The return of λ to λ_s under a constant stimulus (either excitatory or inhibitory) evidences the adaptation of the Ampullae of Lorenzini to DC fields in the water. We measured and characterized the adaptation time constant for those nerve fibers. This is the first time the adaptation time constant has been characterized for the Ampullae of Lorenzini of *Platyrhinoidis triseriata* as far as the published data go.

7.2.2 Adaptation's time constant

We characterized the adaptation time of 13 excitatory responses ($\lambda - \lambda_s > 0$). Each individual response was normalized by the maximum rate of action potentials per second of the nerve ($\lambda - \lambda_s/\lambda_{max}$), and a characteristic curve was obtained by taking an average of all the responses. The time-course of adaptation after an excitatory stimulus has a fast initial decline and then a slow decline. This nerve response is well characterized by a two-exponential function fit, with one fast-decaying exponential and one

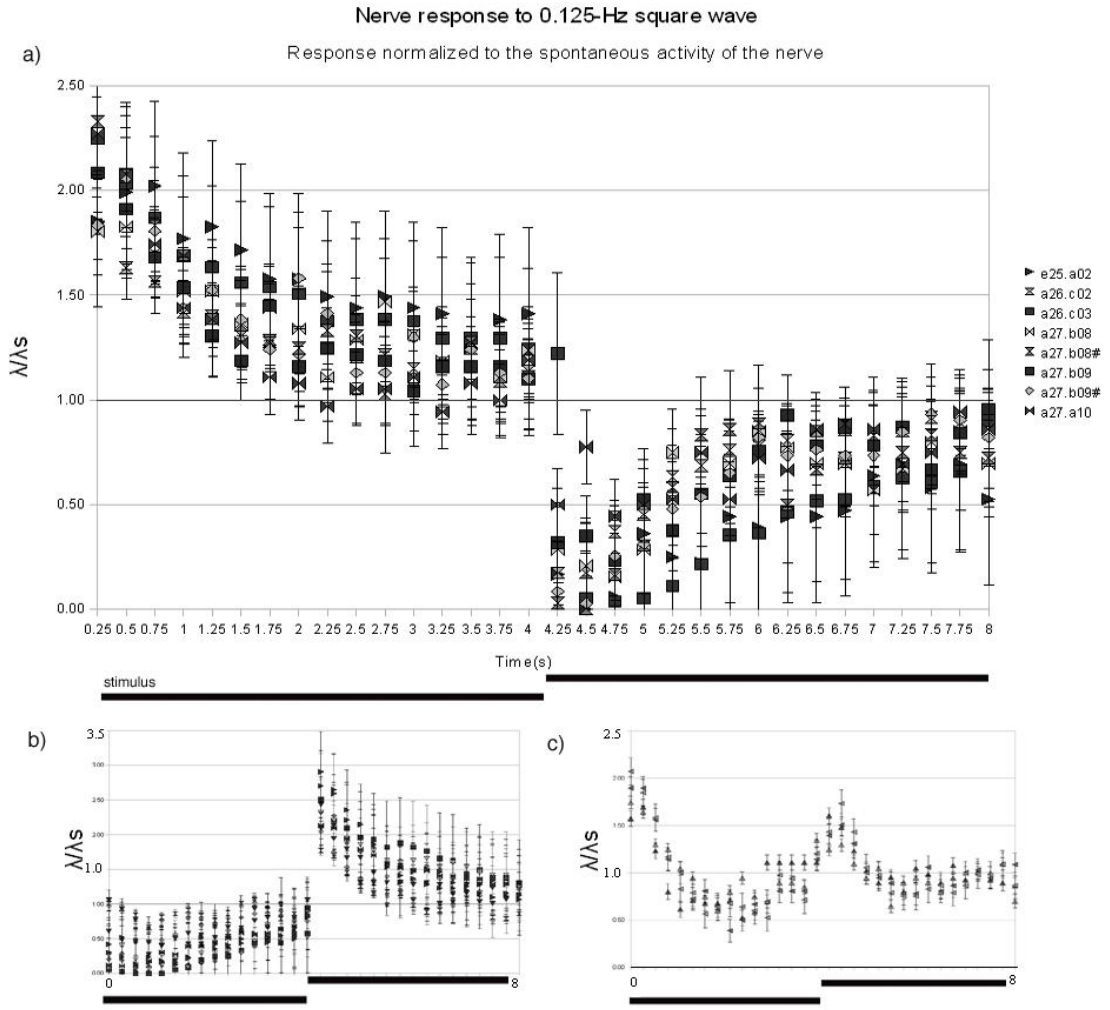

Figure 7.1: Adaptation to constant fields

Response to 0.125-Hz square-wave electric field in the water. Response expressed as the normalized rate of action potentials (λ/λ_s). a) eight nerve fibers had an excitatory response following the onset of the stimulus in the water which rapidly returned to λ_s under constant stimulus, b) ten had an inhibitory response following the onset of the stimulus in the water which returned to λ_s. The change of stimulus polarity after 4 seconds inverted the responses of the nerve fibers. c) Four recordings had an uncommon response with excitatory responses for both stimulus polarities. Onset of negative polarity of the stimulus at t=0. Error bars represent the sample variance.

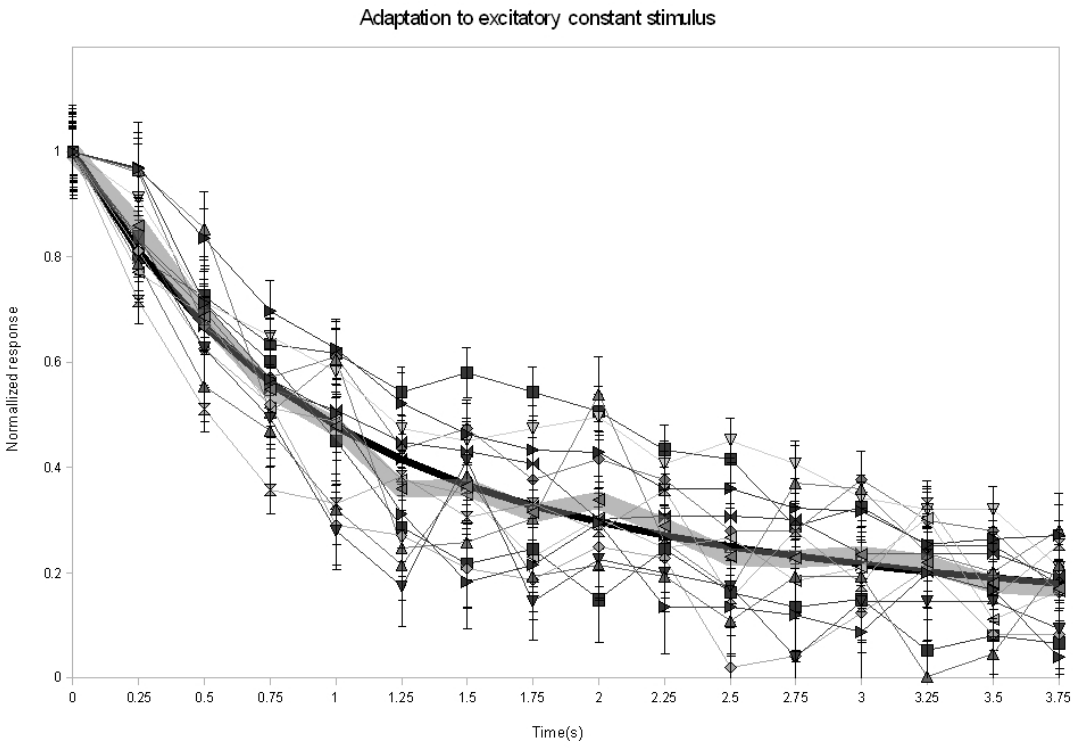

Figure 7.2: Adaptation time constant

Normalized rate of action potentials per second $(\lambda - \lambda_s/\lambda_{max})$, t=0 onset of constant excitatory stimulus in the water. Gray band: average of response from the 13 nerve fibers. Black line: least square fit $y(t) = \alpha \exp(-t/\tau_1) + (1-\alpha)\exp(-t/\tau_2)$. $\alpha = 0.6383$, $\tau_1 = 0.7943$ seconds, and $\tau_2 = 5.1146$ seconds. Error bars represent the sample variance.

slow-decaying exponential: $y(t) = \alpha \exp(-t/\tau_1) + (1-\alpha)\exp(-t/\tau_2)$. The parameters were determined numerically by the least squares method. Local optima were avoided in the minimization by generating a matrix of different initial guesses for the exponential parameters and selecting the fit with smallest norm of the residual. The resulting parameters are $\alpha = 0.6383$, $\tau_1 = 0.7943$ seconds, and $\tau_2 = 5.1146$ seconds. The average time constant of the ampulla, or the time when the response to a constant excitatory stimulus will be 37% of the initial value, is 1.5 seconds (see figure 7.2).

7.3 Response to small sinusoidal stimulus after DC-field adaptation

To test the effect of DC-field adaptation on the linear dynamic range of the ampullae, we measured the threshold of sensitivity and maximum stimulus amplitude with linear response of the organ for 1-Hz sinusoidal fields in different ambient DC electric fields. The results show DC-field adaptation as an effective mechanism to preserve the sensitivity to small varying fields in the presence of strong constant fields. Figure 7.3 shows how the linear dynamic range is preserved by adaptation, shifting the threshold of sensitivity of the nerve above the DC-fields present in the water.

Additionally, we tested the sensitivity of the ampulla in the wide range of electric field strengths the animal may find in the ambient fields of the ocean. Figure 7.4 shows the linear dynamic range of the organ in a wide range of ambient electric field strengths, from less than 80 nV/cm up to 10.2 $\mu V/cm$. The linear dynamic range of response for 1-Hz sinusoidal stimulus was measured with no additional DC field three consecutive times at five minutes intervals, and then measured at DC fields strengths of 320, 640, 1280, 2,560, 5,120 and 10,240 nV/cm. Due to adaptation, the presence of a DC field 32 times bigger than the maximum sinusoidal stimulus with linear response does not saturate the sensory organ. At the same time, a sinusoidal stimulus with amplitude 180 times smaller than the ambient electric field still produces a period histogram with a sinusoidal envelope. Hence, the sensitivity to small sinusoidal stimulus is preserved in the presence of a wide range of ambient DC fields.

7.4 Active control of the range of electric fields sensed by the animal

The DC-field adaptation in the Ampullae of Lorenzini accounts for the sensitivity of a resting animal to small, varying electric fields in the presence of strong constant fields, a very useful feature both for hide-and-wait predatory strategy and to filter the animal's own bioelectric field (see chapter 2). On the other hand, the DC ambient electric fields are of vital importance in navigation and orientation, carrying information about

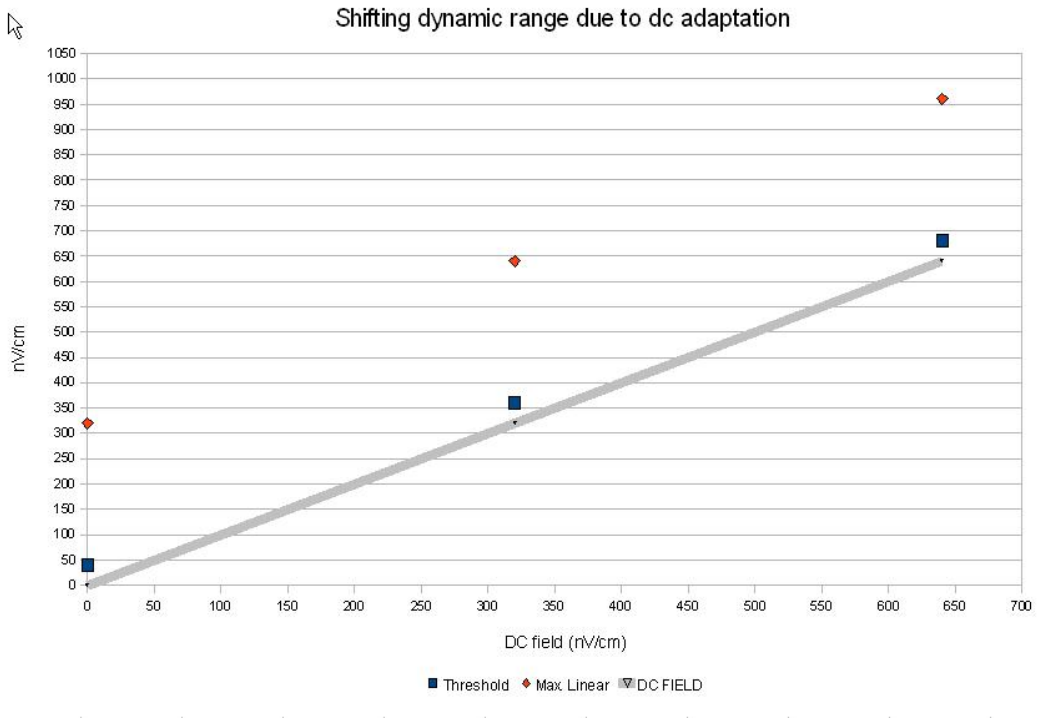

Figure 7.3: Shifting of the Ampulla's linear dynamic range due to adaptation

The abscissa represents the strength of the DC ambient electric in nV/cm and the ordinate shows the fields in the seawater, that is, DC and sinusoidal fields combined in nV/cm. In a resting animal, the response to 1-Hz sinusoidal fields preserve the threshold and maximum amplitude of linear response in the presence of a) no DC field, b) a DC field with a strength equal to the maximum stimulus amplitude of linear response, and c) a DC field with a strength twice the maximum stimulus amplitude of linear response. The threshold and maximum stimulus amplitude of linear response were measured one minute after adding the DC field to allow for the organ's adaptation.

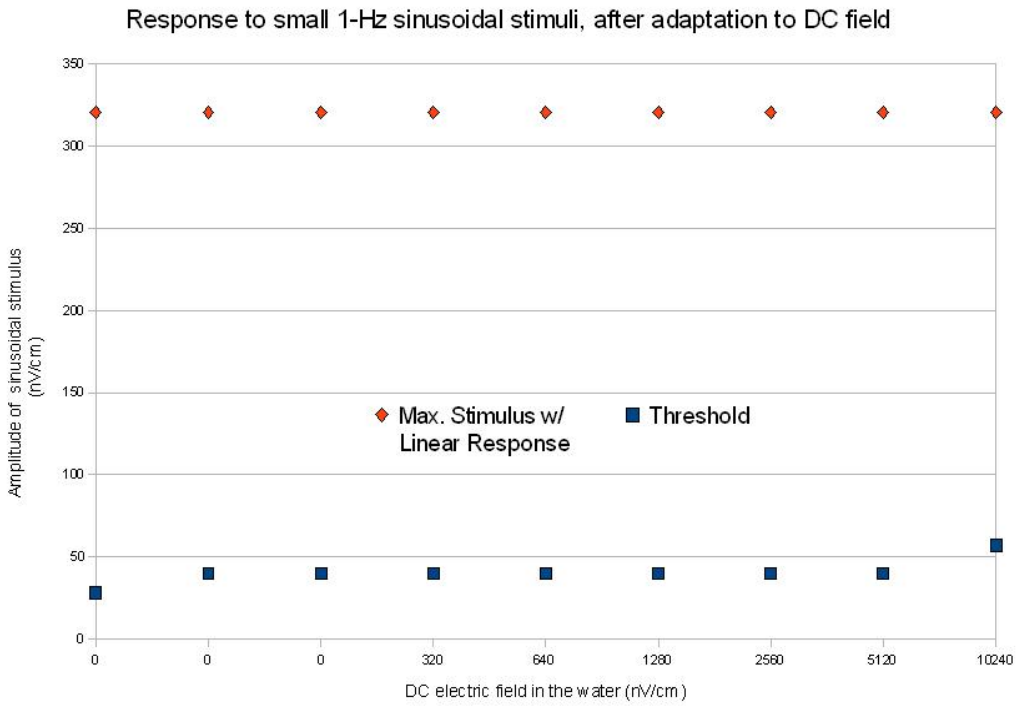

Figure 7.4: Linear dynamic range in the presence of strong constant fields

The abscissa's values represent the strength of the DC ambient electric field in the water and the ordinate shows the linear dynamic range of the organ (not to scale). Adaptation allows the ampullary nerve of a resting animal to carry information about field variations as small as 57.2 nV/cm in the presence of a 10,240 nV/cm DC field.

the ocean currents and tidal flows. The animal takes advantage of the DC electric fields in the water by moving in the field and sensing the effective stimulus before adapting to it. Figure 7.5 shows how a thornback ray can modulate the electric signal it receives by changing its heading with respect to the ambient electric field. Due to the ampulla's adaptation, the effective stimulus for the animal is not the new electric field with respect to the animal's body, but the difference between the new and old electric field.

The animal's swimming introduces electric signals due to the presence of the magnetic field of the earth (see chapter 2). We focus this chapter on the signals related to modulation of the ambient electric field and discuss the induced electric fields in chapter 8. The thornback ray in our experimental setup is resting, therefore it does not modulates the DC electric field in the water. To simulate the electric field experienced by a swimming animal in a horizontal ambient field we use sinusoidal stimuli (see figure 7.5).

7.4.1 Directional response to low-frequency sinusoidal stimulus in the thornback ray

Pore location, canal orientation, canal length, and skin resistance contribute to the effective electric stimulus in the Ampullae of Lorenzini (see chapter 3). Hence, the morphological features of the animal's sensory system have an important role in widening the dynamic range of the electric sense.

As discussed in chapter 1, pore-positive stimuli decrease λ, and pore-negative stimuli increase it. The pore distribution on the ray's skin produces a phase shifting of the response to sinusoidal fields as shown in figure 7.6. An ampulla with its canal oriented parallel to the direction of the sinusoidal stimulus will receive a maximal electric signal. Conversely, an ampulla with its canal oriented perpendicular to the stimulus will receive no signal.

We measured the response to low-frequency sinusoidal electric stimuli of different relative orientation. The ampulla's response shows different thresholds of sensitivity to low-frequency sinusoidal stimuli in two different orientations, parallel and perpendicular to the animal's anteroposterior axis (see table 7.1).

For low-frequency electric fields both the drop across the skin and the internal

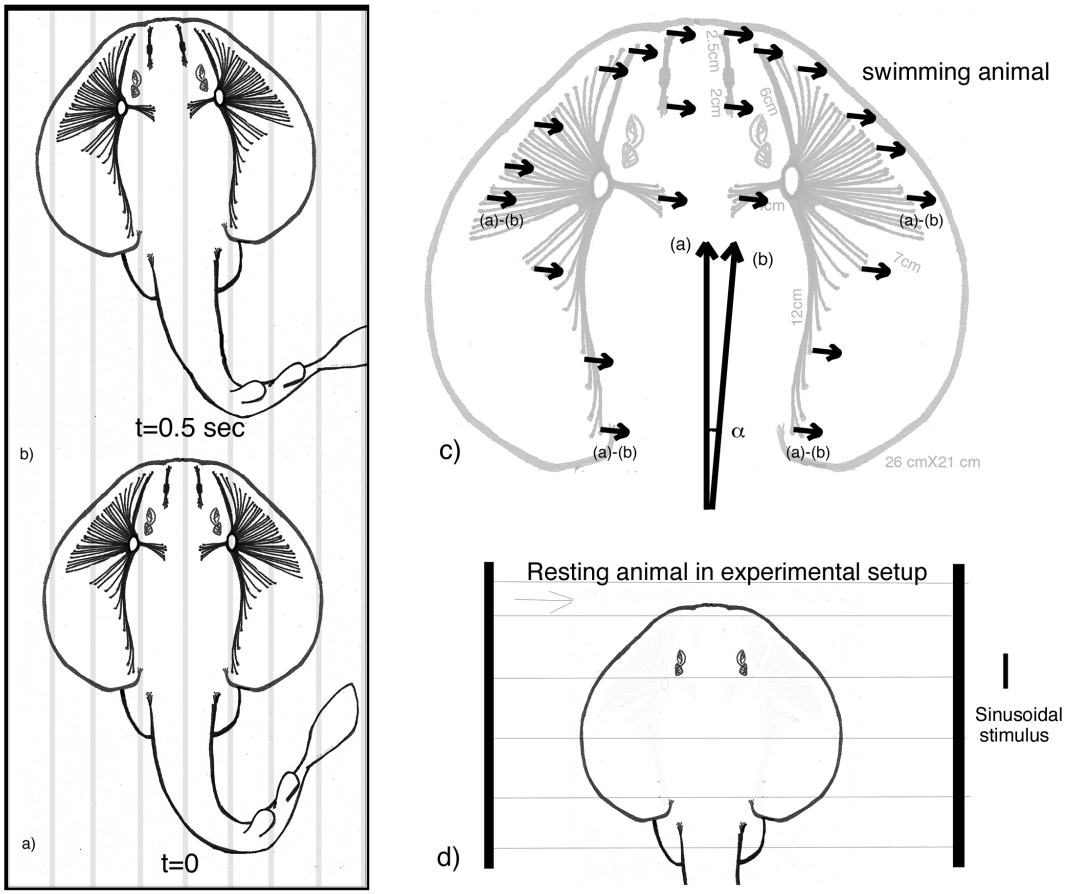

Figure 7.5: Modulation of the ambient electric field

Ray swimming in equatorial waters, in the presence of a DC ambient electric field, a) at time t=0 the ray has already adapted to the ambient field parallel to its anteroposterior axis. b) Without changing its speed, the animal changes heading by a small angle moving counterclockwise in a short time compared to the time constant of adaptation. c) The effective stimulus received by the ray: α represents the rotation of the ray with respect to the electric field. Due to the ampulla's adaptation, the effective stimulus is not the new electric field, but the difference between the old and new field, proportional to $2E\sin(\alpha/2)$. The clockwise-counterclockwise repetition of this behavior produces a sinusoidal effective stimulus perpendicular to the anteroposterior axis of the animal d) A sinusoidal electric field, perpendicular to the animal's anteroposterior axis, simulates the field experienced by a ray swimming in an horizontal ambient electric field mostly parallel to its anteroposterior axis.

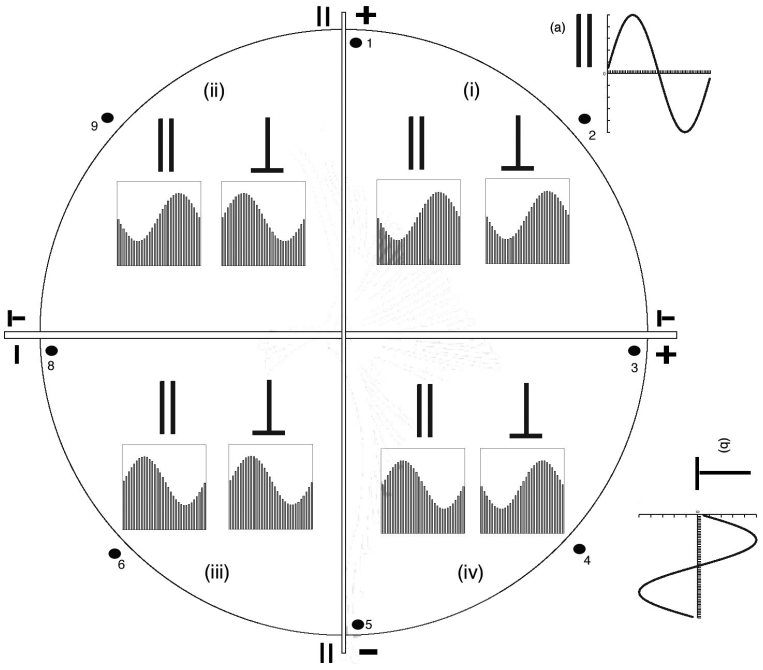

Figure 7.6: Expected period histograms for sinusoidal stimulus

Eight pores located in the circumference with the center of the circle representing the voltage reference. Period histograms marked as ∥ represent the response of organs with pores in the respective middle of the quadrant to stimulus parallel to the line crossing pores 1 and 5, period histograms marked as ⊥ represent the response of organs with pores in the respective middle of the quadrant to stimulus perpendicular to the line crossing pores 1 and 5. Perpendicular (⊥) fields do not produce an effective stimulus for pores 1 and 5, but they produce a maximum response in pores 3 and 4. Parallel (∥) fields do not produce an effective stimulus for pores 3 and 4 but they produce a maximum response in pores 1 and 5.

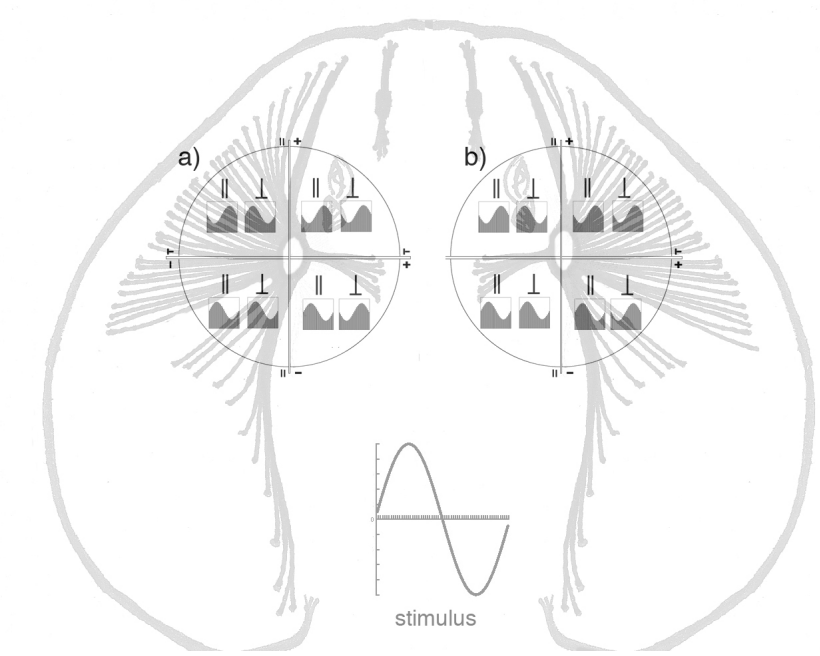

Figure 7.7: Expected phase of response of hyoidal ampullae

Dorsal view of the thornback ray, representation of the expected period histograms for sinusoidal stimulus in the linear range of the electroreceptors from the a) left hyoidal pores and b) right hyoidal pores. Pores en each side located in four different quadrants with the center of the located in the hyoid capsule. Conventions as in figure 7.6. Note the asymmetry between left and right medial hyoidal regions and left and right lateral hyoidal regions.

Table 7.1: Different linear dynamic range for 1-Hz sinusoidal stimulus fields parallel (∥) and perpendicular (⊥) to the anteroposterior axis of the animal.

nerve fiber	Stim.	Threshold nV/cm	Max. Stimul. Linear nV/cm	Linear Range (dB)	Quadrant (Fig. 7.7)	Angle respect medial line
a	⊥	320	2,548	18	(i)	79.92
	∥	57	453	18		
b	⊥	114	902	18	(iv)	-5.08
	∥	1,277	3,599	9		
c	⊥	114	902	18	(iv)	-14.07
	∥	453	2,548	15		

voltage gradients contribute to the effective stimulus. Figure 7.7 may be used with caution to identify the quadrant where one ampulla's pore comes from, because it assumes the voltage of the capsule is the same as on the skin above it (see chapter 3).

As an exercise to confirm the directional response of the ampulla, we calculated pore location using the nerve fiber response to parallel and perpendicular fields. The radial angle was calculated using the threshold of sensitivity for each stimulus orientation: $\theta = \arctan(\text{threshold } \perp / \text{threshold } \parallel)$. To disambiguate the respective quadrant for each pore, we obtain the sinusoidal envelope of the period histogram of the response and compare it with figure 7.7. The results of predicted pore location and canal orientation were plotted side by side for three pore locations determined experimentally using a local stimulus probe (see figure 7.8). The ratios of the thresholds of sensitivity of three nerve fibers recorded are an adequate predictor for the location of the three pores on the dorsal skin of the animal.

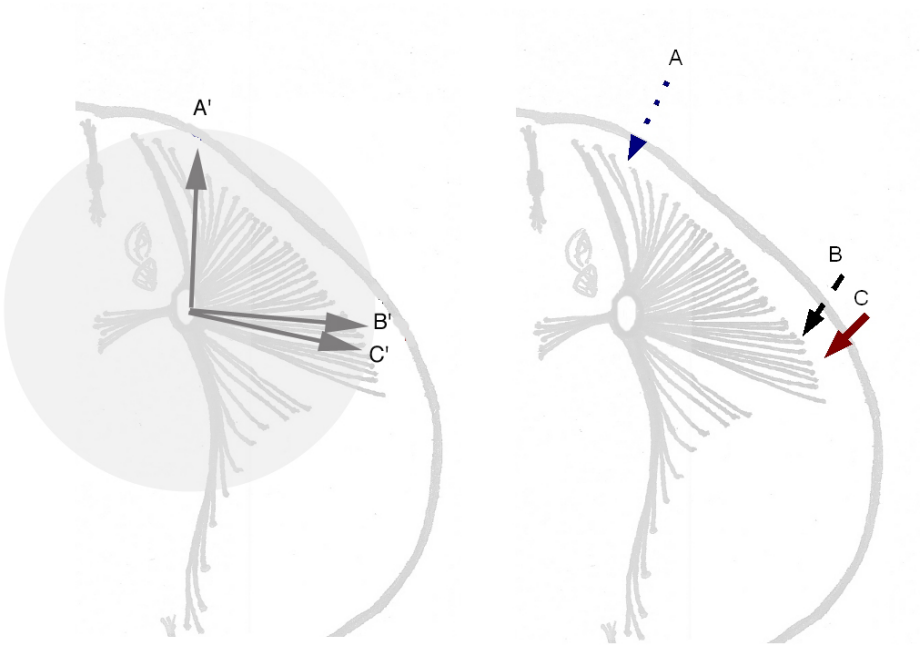

Figure 7.8: Predicted pore location using the recorded threshold of sensitivity

Calculated pore location using the nerve fiber response to sinusoidal fields parallel ($\parallel$) and perpendicular ($\perp$) to the anteroposterior axis. Values in table 7.1. The positions of the pores were directly measured and plotted in the right side of the picture for comparison.

8

Discussion

8.1 Adaptation of the sense organs

The observed DC-field adaptation of the ampulla of *Platyrhinoidis triseriata* is in harmony with the common wisdom of the scientific field. In 1965, R. W. Murray [40] described the adaptation of the mandibular ampullae of *Raja ocellata* to DC currents stimulating the ampullary pore. Since then, adaptation to constant fields was accepted as a characteristic shared by all Ampullae of Lorenzini, and little subsequent effort was made to characterize it in other species, except for the Black Sea ray, *Trigon pastinaca* [1]. Murray found that the rate of action potentials per second will adapt half way ($\lambda - \lambda_s = 1/2\ \lambda_{max}$) in about 3-5 seconds. We found the time constant of adaptation for *Platyrhinoidis triseriata* to be 1.5 seconds, with a half-way adaptation time of 1 second. The difference may be accounted for by species variability, but the methodology was also different. While Murray used a set constant current to stimulate the pore, we were able to refine our stimulus to be at the top of the linear dynamic range for each nerve fiber.

8.2 Adaptation as a mechanism allowing a wide linear range of operation in a resting animal

The measurement and characterization of the adaptation of the Ampullae of Lorenzini of the thornback ray give us a new insight into the linear dynamic range of the organ. The Ampulla of Lorenzini shifts its linear dynamic range by adapting to ambient

constant fields, allowing sensitivity to small varying electric fields in the presence of a wide range of constant field strengths. Adaptation becomes the fundamental physiological mechanism to explain the widening of the dynamic range of operation of the electric sense of a resting thornback ray.

8.3 DC adaptation as a mechanism allowing a wide linear range of operation in a swimming animal

As useful as the DC-field adaptation is both for hide-and-wait predatory strategy and to filter the animal's own bioelectric field, its usefulness is small compared to the role of adaptation in electric-field modulation. Due to the ampulla's adaptation, the effective stimulus for a swimming animal is no longer the configuration of the electric potentials on the skin at any given time, but the difference between the electric configuration at the time t and the electric configuration at time $t - \Delta t$, with Δt smaller than the adaptation time.

Figure 7.5 shows how the thornback ray swimming in a moderate swerve modulates the strength of the effective stimulus produced by the ambient electric field. By allowing enough time to adapt to the ambient electric field and then changing its heading by a small angle α, the animal modulates the effective stimulus strength by a factor of $sin(\alpha/2)$. Hence, through controlled movement, the animal is capable of actively modulating the ambient electric field to yield an effective stimulus with a strength in the linear range of its sense organs. The direction of the effective stimulus in this case is almost perpendicular to the ambient electric field ($\theta = 90 - \alpha/2$) and the clockwise-counterclockwise repetition of this behavior produces a horizontal sinusoidal field perpendicular to the anteroposterior axis of the animal.

8.3.1 Effect of the ampulla's length and orientation

A careful anatomical exploration of the thornback ray shows that ampullae from the same capsule have specific pore distributions, covering a wide range of canal orientations and lengths (see chapter 3). The animal's morphology gives each ampulla a different response to a external stimulus, with a linear relationship between the response

of the ampulla and the projection of the ampullary canal on the direction of the homogeneous electric stimulus [7]. Hence, ampullae show little response when the projection of the electric stimulus on their canal is very small, either by having a short canal or by being perpendicular to the direction of the stimulus, while other ampullae may show a large response by having a long canal and being parallel to the direction of the stimulus. The key point to understand regarding canal geometry and dynamic range of the electric sense is that the direction and strength of effective stimulus is not the direction and strength of the constant ambient electric field, but rather the direction and strength result of behavioral mechanisms and receptor adaptation, which maintain the effective stimulus within the linear dynamic range of the ampullae.

8.4 A thornback ray swimming in the ocean

A thornback ray swimming near the surface in an ocean current may sense an existing uniform horizontal electric field and receive unambiguous information about its magnetic heading [29]. Starting by maintaining a constant speed to allow time for adaptation, the ray can then either veer left or right, preferably at a constant speed to avoid the left-right electric fields generated by interaction with the vertical component of the magnetic field (see chapter 2). If the strength of the resultant field does not provide an adequate stimulus for the ampullae, the animal may explore the field again, changing its heading in a more abrupt way to increase the amplitude of the resulting stimulus, or to the contrary reducing the movement to a slight turn of the disk to decrease the amplitude of the resulting stimulus. The resultant stimulus and the directional response of the Ampullae of Lorenzini give unequivocal information about the direction of the ambient electric field. The amount of rotation in relation to the effective stimulus provides information about the strength of the ambient field. When the animal increases its speed without changing its heading the ampulla effectively filters the information from the ambient electric field and receives information about its magnetic heading.

8.5 Recommendations for further research

Little is know about the role of the ampulla's multiple afferent innervation in the electric sense of sharks and rays. A staggered sensitivity of the nerve fibers is a plausible mechanism to widen the linear dynamic range of the ampulla by keeping some insensitive nerve fibers from saturating even in the presence of very strong stimulus strengths, while allowing some nerve fibers to be very sensitive for operation in the lower end of the sense's dynamic range. On the other hand, the role of multiple afferent innervation may be to reduce the noise from the ampulla's sensory transduction and synaptic transmission by averaging the response of all the afferent nerve fibers of the sense organ. The setup at the Sensory Biophysics Laboratory offers the unique advantage of simultaneously measuring two nerve fibers located at very close proximity to each other. Because five to ten tightly-packed nerve fibers innervate the ampulla and travel in very close proximity in the cranial nerves of the animal, this setup offers an ideal tool for the comparative study of the response of two nerve fibers coming from the same ampulla. The argument that increased signal-to-noise ratio in the ampulla may have higher biological relevance than the pursue of a wider linear range in a single sense organ calls for an experimental study to clarify the function of the ampulla's multiple innervation.

8.6 In conclusion

We propose that the adaptation to constant stimuli and directional response of the ampullae in combination with the described behavioral mechanisms, allow the animal to extend its electroreceptor's linear dynamic range of operation in the wide range of electric field strengths in the ocean.

A

Appendix: Electrical Properties of Seawater

A.1 Conductivity of seawater at different frequencies

For an electrolyte, such as seawater, the electric conduction is due to an ionic flow. Applied DC electric fields in the solution will force the ions to accelerate, and the viscous forces in the liquid will oppose the movement. As a result, the initial acceleration is followed by a steady state, with ions moving at constant velocity. The concentration and size of the ions, together with the temperature of the electrolyte will determine the conductivity.

In seawater exposed to low-frequency AC electric fields, the ions in the liquid will start moving, increase their speed, then reduce their speed, stop, start moving in the opposite direction, increase their speed, then reduce their speed, stop and repeat the cycle again, following the driving force of the field. For higher frequencies, the cycle will be shorter, and the ion movement will be reduced, and eventually the dielectric current prevails. For frequencies of the order of 10 GHz the dipole moment of the water molecule aligning with the electric field will result in an effective movement of the oxygen and hydrogen back and for. In the same fashion, for higher frequencies the electrons in the ions will displace with respect to their positive nucleus, generating an electric current. The elastic electrical forces that hold the atoms and molecules together,

and not viscosity, are the forces opposing this current.

If we impose a DC electric field in seawater by means of two electrodes, we will observe a current passing between the positive electrode (anode) and negative electrode (cathode) . Negative ions (anions) such as chloride, will move towards the anode, and positive ions (cations) such as sodium will move towards the cathode, and the combination of those two opposite flows together constitute the observed electric current in the water.

A net electric force opposed by viscous forces will produce a steady state movement of charges in the seawater, and therefore an electric current inside an ohmic media. These currents generate voltage gradients along their path according to ohm's law, and it is the measurement of the voltage gradient between two points in the water what provides the information about the electric fields in the aqueous environment.

A.2 Conductivity dependence on temperature

The electric conductivity for DC fields in seawater with salinity of 35 ppt at sea level follows this empirical function of temperature:

$$\begin{aligned}
\sigma(35,T) &= \sigma(35,15)(c_0 + c_1T + c_2T^2 + c_3T^3 + c_4T^4) \qquad \text{(A.1)}\\
c_0 &= 6.766097X10^{-}1\\
c_1 &= 2.00564X10^{-}2\\
c_2 &= 1.014259X10 - 4\\
c_3 &= -6.9698X10 - 7\\
c_4 &= 1.0031X10 - 9\\
\sigma(35,15) &= 0.043\frac{S}{cm}
\end{aligned}$$

A practical way to produce DC electric fields in the seawater requires a current source connected to two electrodes. Assuming seawater of constant salinity (35 ppt)

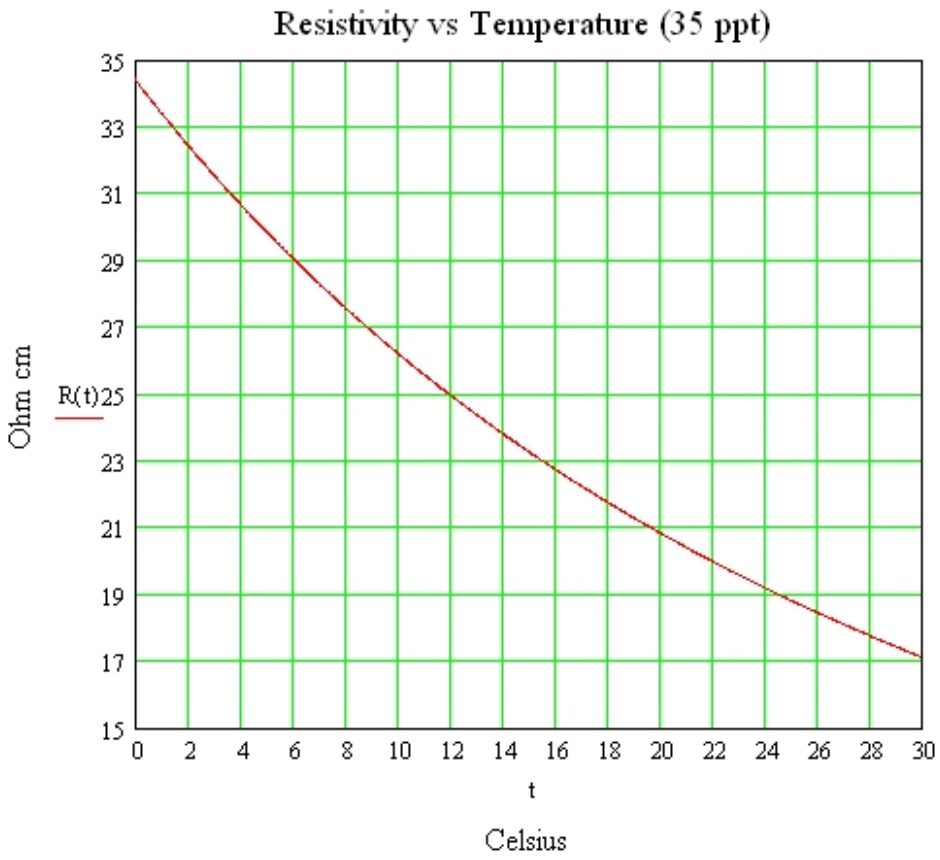

Figure A.1: Resistivity vs Temperature at 35 ppt

and constant cross-section of know value, the graph A.1 can be used to calibrate the amplitude of the electric field under different water temperatures.

B

Appendix: Electromagnetic Induction and Ray's Magnetic Orientation

B.1 Electromotive forces in a channel

Imagine a seawater channel surrounded by non-conductive rock in the Southern hemisphere, and let the channel run across the continent from west to east, and let the flow of water be in the same direction. The electromotive force induced by the movement of the seawater in the magnetic field of the earth could be decomposed in two components, one vertical electromotive force induced by the movement in the horizontal component of the magnetic field, and one horizontal electromotive force induced by the movement in the vertical component of the magnetic field.

The electromotive force perpendicular to the surface of the earth will move the anions towards the surface of the water and the cations towards the bottom of the channel. Those charges will accumulate at the surface and bottom of the channel generating and electric field opposing the movement of charges, quickly reaching a point when the charge accumulation counteracts the electromotive force, and there is no electric current from the surface to the bottom. The electromotive force parallel to the surface of the earth will move the anions towards the north boundary of the channel and the cations

towards the south boundary of the channel, getting to a similar charge accumulation and a resultant null electric current between the boundaries. This situation gives rise to zero net force in the water. A pair of electrodes drifting with the water will measure no voltage gradient between them, on the other hand, a pair of electrodes fixed in the boundaries of the channel will measure the electric field due to charge accumulation in the boundaries, because they are not exposed to the electromotive force.

Next, allow the rock to be conductive. There is no electromotive force in the rock, being at rest in the magnetic field of the earth, but the charge accumulation at the boundary of the channel generates an electric field forcing the cations to move towards the north and the anions towards the south in the conductive rock, reducing the accumulation of charge in the boundary and allowing the continuous passage of electric current in the channel and the surrounding rock. In this situation we have a net force acting on the ions due to the reduction of the charge accumulation, and therefore a measurable electric field in the water. The voltage gradient measured by a pair of drifting electrodes is then different than zero, and the voltage gradient measured with a pair of fixed electrodes is smaller than the one measured in a non-conductive boundaries. For an oceanic current that is completely short circuited by the boundaries, the drifting electrodes will measure a voltage gradient generated by the induced electric current, and fixed electrodes will measure no voltage gradient.

B.2 Electric fields of a wind-driven ocean current

In the ocean, the boundaries of the hypothetical channel are replaced by the seawater adjacent to the channel, as in the case of wind-driven surface currents. The water adjacent to the ocean current is not necessarily at rest in the magnetic field of the earth. Hence, the electric return path can be moving or at rest in the magnetic field, having its own associated electric fields depending on its own velocity and conductivity of the boundaries. Therefore, induced electric currents associated with the water movement constitute relevant signatures of the ocean currents, but the interpretation of the measurements of a drifting pair of electrodes requires the understanding of the environmental conditions before been able to determine the velocity of the ocean current

with respect to the bottom.

B.3 Electromotive forces in a swimming ray

For the sharks and rays moving in the earth's magnetic field, the electromotive force acting on them is nothing else than an electric field. Hence, their electric sense gives them the ability to orient in the magnetic field of the earth. The classical description of the field experienced by the animal is similar to the described for electric fields of ocean currents. The seawater around elasmobranch fishes has very low resistivity compared to the body of the animal, hence, there is a near-maximal electric current density $\overrightarrow{J}$ flowing across the animal and back trough the seawater. The electric field $-\rho\overrightarrow{J}$ is then almost equal to $\overrightarrow{v} \times \overrightarrow{B}$ in the body tissue ($\overrightarrow{v} \times \overrightarrow{B} - \rho\overrightarrow{J}_{body} \approx 0$).

A differential pair of ampullae parallel to $\overrightarrow{v} \times \overrightarrow{B}$, act as a high-ohmic voltmeter ($-\rho\overrightarrow{J}_{ampulla} \approx 0$). The sensory epithelium in the ampullae proper will experience the full extent of the induced field, with the effective stimulus being the voltage gradient integrated along the ampullary canals.

In the case of a ray swimming towards the east in equatorial waters, a ventro-dorsal force is experienced. An animal swimming towards the west experiences a dorso-ventral force and an animal swimming towards the south or north will experience no force. In other latitudes, the vertical component of the magnetic field of the earth introduces forces in the plane of the ray's disk, perpendicular to the velocity of the animal. Those forces are right-left in the northern hemisphere and left-right in the southern hemisphere.

C

Appendix: The Ampullary Simulator

C.1 Description of the ampullary simulator

This dual electric-signal-to-impulse-rate converter consists of two ampullary simulators. Each unit has independent controls for the different variables of the rate of impulses per second of the spontaneous activity and the response to stimulus. To be consistent with the experimental setup it has a shared amplitude noise (simulating the noise from the recording electrode) and receives the same stimulus in both units. The ampullary simulators can run independently, or one simulator will trigger the other to study overlapping impulses. The simulator reached such a degree of usefulness as an heuristic tool that it has been made a permanent part of the setup for testing and educational purposes.

C.2 Implementation of the ampullary simulator

The ampullary simulator is an analog-signal-to-impulse-rate converter with rate and amplitude noise sources. It generates electric impulses in the fashion of action potentials, at a rate that can be set to a number of impulses per second. A noise source controls the impulse rate to model the natural jittering in the spontaneous activity rate of the nerve fiber. The impulse rate is also controlled by a voltage input, to model the

change of action potential rate due to electric stimulus of the ampulla. A second noise source is added to the impulses to model the noise introduced by the recording electrode and setup.

A voltage-controlled function generator is the source for ramp-shaped signals filtered with a high-pass passive filter to produce impulses. The frequency dial is set to 30 Hz to simulate the rate of 30 I/s present in the afferent nerves of healthy thornback rays in seawater at 15℃. The noise sources are resistances attached to amplifiers. To simulate the electrode noise we mix the output of the function generator with a noise source. This output connects to a switch at the input of the data acquisition setup. In one position of this switch, the setup connects to the ampullary simulator, in the other position it connects to the pre-amplifier used for the electrode recordings. The signal from the stimulus generator of the electrophysiological setup is filtered with an active low-pass filter to simulate the decreased response to frequencies higher than 8 Hz. This signal is mixed with the output of one noise source and connects to the voltage control of the function generator.

D

Appendix: The Two-unit Action Potential Sorter

D.1 Sorting criteria in the two-unit action potential sorter

The custom-made action potential sorter takes advantage of recordings where only two action potential trains are above background noise and their amplitude is distinct enough to be separated electronically. In that case, one miniature suction electrode carries simultaneously two action potential trains, either the nerve activity of two ampullae, or the nerve activity of two afferent nerve fibers from the same ampulla.

The difficulty of two-unit recording analysis is to sort which action potential belongs to one fiber and which to the other. Even when one unit has an amplitude big enough to be separated from the other by traditional window discriminator techniques, the overlapping impulses have highly-variable amplitudes and the coinciding pulses create one giant action potential, making window discrimination unreliable (see figure 5.2).

The action potential sorter has a simple criterion for determining overlapping of impulses from two nerve fibers. It uses a time window just shorter than the refractory period in a single nerve fiber. This window is triggered every time a first impulse is received and looks for impulse arrivals during that time window, if an action potential arrives during that time, they are detected as overlapping impulses. The criterion for coinciding impulses is determined by a window discriminator with the trigger level higher

than the maximum regular amplitude of the large-amplitude train.

D.2 Conditioning of the signal

The output from the suction miniature electrode is clipped at a level selected by the user, to cut any background activity and passing only impulses from the two nerve fibers of interest. Additionally, the signal is integrated with a running integrator at a set time window of integration. That produces impulses that have the same time width and also improves the separability of the impulses using window discriminators.

D.3 Separation using window discriminators

We sort the conditioned signal using two window discriminators. One window discriminator is set to have only the small-amplitude impulses inside the window, and the large-amplitude impulses above the window, this discriminator then will miss the small-amplitude impulses during coincidence and sometimes miss or double-count them during overlapping. The other discriminator has the threshold levels to detect only impulses that are bigger than the regular large-amplitude impulses.

D.4 Custom made box

The custom made box regulates the integration time for the conditioning of the signal, and also the time window for the overlapping detection. Additionally, it mixes the output of the the window discriminators with the coincidence and overlapping detection. When there is a coincidence it adds a pulse to the train of small-amplitude pulses, and when there is an overlapping, it adds a pulse to both pulse trains, overriding the output of the window discriminator for the duration of the overlapping.

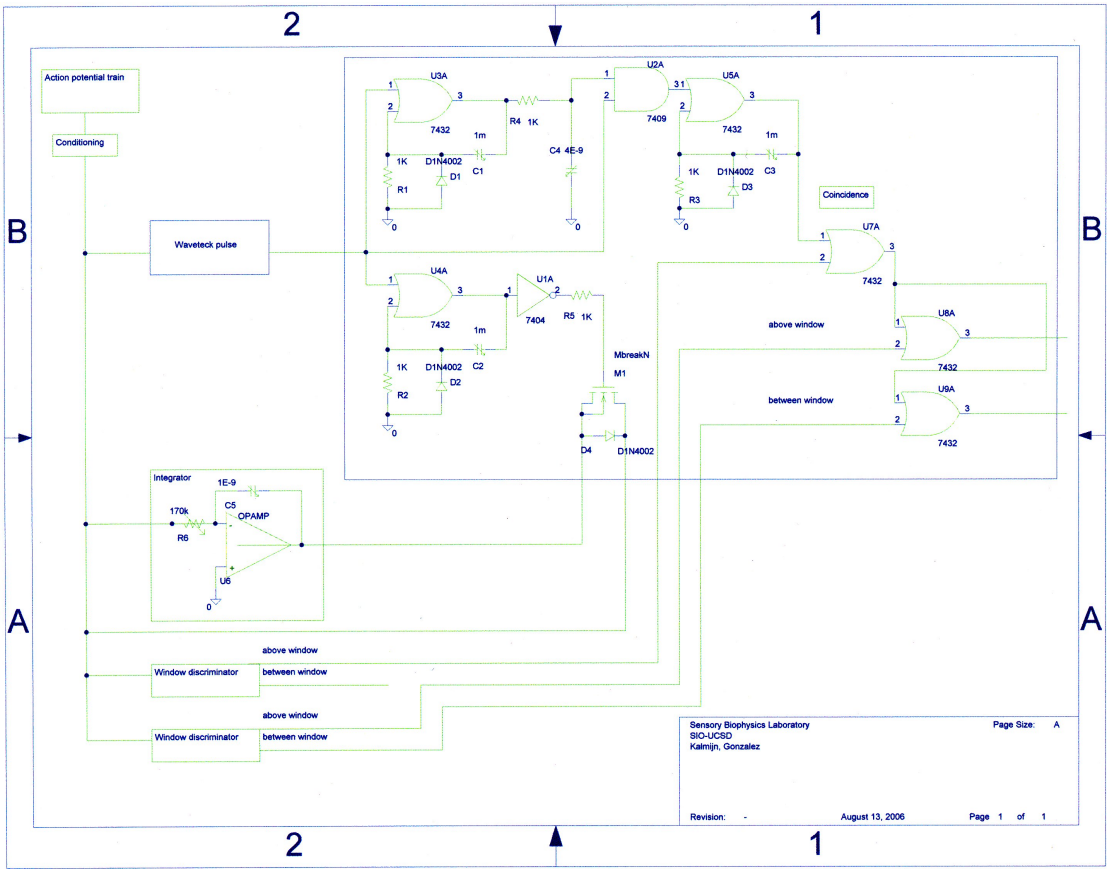

Figure D.1: Schematic diagram of action potential sorter

E

Appendix: Ray Ringer Solution

E.1 Elasmobranch's blood composition:

Elasmobranch fishes retain high concentrations of urea and NaCl in their blood for osmotic regulation in the seawater environment. Urea may account for about one-third of the solute particles in elasmobranch blood [14]. The blood urea nitrogen ranges from 750 mg.% to 1100 mg.% in samples from *Mustelus canis* and from 870 mg.% to 1320 mg.% in samples from different species of *Raja*. For thornback rays, the normal values of blood composition are reported in table E.1:

For the preparation of a Ringer solution suitable for use in thornback ray we used normal values of inorganic solutes reported by Urist [48]. The ionic strength calculated for phosphate-free physiologic shark solutions is 0.3 M.

E.2 Ray Ringer solution preparation:

a) Mix three solutions from table E.4 in equal proportions

b) Add HEPES (1.787 g / 1,500 l)

c) Adjust for solution pH 7.4

Table E.1: Ion composition of blood of *Platyrhinoidis triseriata*. Values in milliequivalents per liter (meq./L) and milligarms per cent (mg.%), from [48]

Component		Plasma (meq./L)	Red blood cells (meq./L)	Plasma (mg.%)	Serum (mg.%)
Sodium	Na^+	234	20	-	-
Potassium	K^+	11.4	175.2	-	-
Total Calcium	Ca^{++}	10.5	3.4	17.4 ± 2.4	18.2 ± 1.5
Magnesium	Mg^{++}	9.1	7.0	-	-
Chloride	Cl^-	208	160.4	-	-
Bicarbonate	HCO_3^-	3.2	-	-	-
Inorganic P.		3.8	13.4	4.8 ± 0.7	4.2 ± 0.6
Total P.		27	77.4	14.0 ± 3.2	-
Urea (N)		-	-	901 ± 104	

Table E.2: Different Ringer's solution compositions for *Raja erinacea, Raja ocellata*, and *Platyrhinoidis triseriata*. Values in mM.

Solution:	Ra 1 Clusin [8]	Ra 2 Malchow [35]	Ra 3 Goldstein [15]	Pl 1 Fields [12]
$Urea$	415	360	350	315
$NaCl$	340	250	280	300
$Glucose$	0	10	5	5
$NaHC0_3$	2.5	20	8	2.5
KCl	6	6	6	4
$CaCl_2$	1.8	4	5	2
$MgCl_2$	2.5	1	3	2
NaH_2PO_4	0	0.2	1	0
Na_2SO_4	0	0	0.5	0
$HEPES$	5	5	?	7.5
$Trimethylamine$ $n-oxide$	0	0	0	76
Final pH	7.4	7.6	?	7.3

Table E.3: Ray ringer solution composition.

Ingredient	Amount (mM)	Molecular Weight	Weight (g) for 1,500 l
$Urea$	415	60.06	37.387
$NaCl$	340	58.44	29.804
KCl	6	74.56	0.671
$MgCl_2$ 6H2O	2.5	203.31	0.762
$NaHCO_3$	2.5	84.01	0.315
$CaCl_2 2H_2O$	1.8	147.03	0.397
HEPES			

Table E.4: Stock Solutions composition for a 500 ml volume.

Solution	Ingredients	Amount
SS 1	$NaHCO_3$	0.315 g
SS 2	$Urea$	37.387 g
	$NaCl$	29.804 g
	KCl	0.671 g
	$MgCl_2 6H_2O$	0.762 g
SS 3	$CaCl_2 2H_2O$	0.397 g

F

Appendix: Least Squares Fit: Analytic Solutions and Intermediate Steps

F.1 Non-linear regression

The assumption intrinsic to this analysis is a linear response of the nerve fiber to the appropriate stimulus in the tank, hence a sinusoidal stimulus will be express in the period histogram as sinusoidal envelope of the bins. We use non-linear regression to fit an envelope to the data in the period histogram. The resultant sinusoidal function is then called the "response of the nerve" to a sinusoidal stimulus.

The function $Y(x) = b_0 + b_1 \sin(x + b_2)$, of arbitrary elevation, amplitude, and phase, represents the best fit to the sinusoidal response of the nerve. The parameters $b_0,\ b_1\ ,\ b_2$ are found numerically using the least squares method.

From the histogram data, we can construct the series Y, where each one of the points correspond to the value of the function $Y(x)$ evaluated in each bin.

$$Y_i = b_0 + b_1 \sin(x_i + b_2)\ , with\ i\ =\ 1,\ \ldots,\ N \tag{F.1}$$

$$x_i = \frac{2\pi}{N} i \tag{F.2}$$

We define the value D, representing the sum of the squares of all the differences between the data and the points following the sinusoidal Y.

$$\begin{aligned} D &= \sum_{i=1}^{N} (y_i - Y_i)^2 \\ D &= \sum_{i=1}^{N} (y_i - b_0 - b_1 \sin(x_i + b_2))^2 \end{aligned} \tag{F.3}$$

For D to be a minimum, the following conditions should be true:

$$\frac{\partial D}{\partial b_0} = 0, \qquad \frac{\partial D}{\partial b_1} = 0, \qquad \frac{\partial D}{\partial b_2} = 0 \tag{F.4}$$

Minimizing the expression F.3 and using conditions F.4 results in a set of three equations and three unknowns. Solving the equations for b_0 we have:

$$\begin{aligned} \frac{\partial D}{\partial b_0} = \sum_{i=1}^{N} 2(y_i - b_0 - b_1 \sin(x_i + b_2))(-1) = -2 \sum_{i=1}^{N} y_i + 2 \sum_{i=1}^{N} b_0 \\ + 2 \sum_{i=1}^{N} b_1 \sin(x_i + b_2) \end{aligned} \tag{F.5}$$

Therefore:

$$\begin{aligned}\sum_{i=1}^{N} y_i &= \sum_{i=1}^{N} b_0 + b_1 \sum_{i=1}^{N} (\sin x_i \cos b_2 + \cos x_i \sin b_2) \\ &= \sum_{i=1}^{N} b_0 + b_1 \cos b_2 \sum_{i=1}^{N} \sin x_i + b_1 \sin b_2 \sum_{i=1}^{N} \cos x_i\end{aligned} \tag{F.6}$$

Replacing the values of x_i from the histogram (equation F.2) and separating equation F.6 in its different components:

$$\begin{aligned}\sum_{i=1}^{N} \sin x_i &= \sum_{i=1}^{N} \sin(\frac{2\pi}{N} i) = \sum_{i=1}^{\frac{N}{2}} \sin(\frac{2\pi}{N} i) + \sum_{i=\frac{N}{2}+1}^{N} \sin(\frac{2\pi}{N} i) \\ &= \sum_{i=1}^{\frac{N}{2}} \sin(\frac{2\pi}{N} i) + \underbrace{\sum_{j=1}^{\frac{N}{2}}}_{j=i-\frac{N}{2}} \sin(\frac{2\pi}{N}(j + \frac{N}{2})) \\ &= \sum_{i=1}^{\frac{N}{2}} \sin(\frac{2\pi}{N} i) + \sum_{j=1}^{\frac{N}{2}} [\sin(\frac{2\pi}{N} j) \cos\pi + \cos(\frac{2\pi}{N} j) \sin\pi] = 0\end{aligned} \tag{F.7}$$

$$\begin{aligned}\sum_{i=1}^{N} \cos x_i &= \sum_{i=1}^{N} \cos(\frac{2\pi}{N} i) = \sum_{i=1}^{\frac{N}{2}} \cos(\frac{2\pi}{N} i) + \sum_{i=\frac{N}{2}+1}^{N} \cos(\frac{2\pi}{N} i) \\ &= \sum_{i=1}^{\frac{N}{2}} \cos(\frac{2\pi}{N} i) + \underbrace{\sum_{j=1}^{\frac{N}{2}}}_{j=i-\frac{N}{2}} \cos(\frac{2\pi}{N}(j + \frac{N}{2})) \\ &= \sum_{i=1}^{\frac{N}{2}} \cos(\frac{2\pi}{N} i) + \sum_{j=1}^{\frac{N}{2}} [\cos(\frac{2\pi}{N} j) \cos\pi - \sin(\frac{2\pi}{N} j) \sin\pi] = 0\end{aligned} \tag{F.8}$$

Then equation F.6 can be expressed as:

$$\sum_{i=1}^{N} b_0 \ + b_1 \cos b_2(0) \ + b_1 \sin b_2(0) = \sum_{i=1}^{N} y_i \tag{F.9}$$

And finally:

$$b_0 \sum_{i=1}^{N} 1 = \sum_{i=1}^{N} y_i \tag{F.10}$$

The average number of action potentials per bin is:

$$\bar{y} \ = \ \frac{1}{N} \sum_{i=1}^{N} y_i \tag{F.11}$$

Therefore :

$$b_0 \ = \ \bar{y} \tag{F.12}$$

Because b_0 is simply the average value of actions potentials per bin, the equation F.3 can be rewritten as:

$$\begin{aligned} D &= \sum_{i=1}^{N} (\tilde{y}_i - b_1 \sin(x_i + b_2))^2 \\ \tilde{y}_i &= y_i - \bar{y} \end{aligned} \tag{F.13}$$

Minimizing the expression F.13 using conditions F.4 and solving for b_1 we have:

$$\sum_{i=1}^{N} 2(\tilde{y}_i - b_1 \sin(x_i + b_2))(-\sin(x_i + b_2)) \;=\; \sum_{i=1}^{N} 2(-\tilde{y}_i \sin(x_i + b_2) + b_1 \sin^2(x_i + b_2)) \;=\; 0 \tag{F.14}$$

$$\sum_{i=1}^{N} -2(\tilde{y}_i(\sin x_i \cos b_2 + \cos x_i \sin b_2) - b_1(\sin x_i \cos b_2 + \cos x_i \sin b_2)^2) \;=\; 0 \tag{F.15}$$

$$\begin{aligned} 0 = \sum_{i=1}^{N} & -2\tilde{y}_i(\sin x_i \cos b_2 + \cos x_i \sin b_2) + 2b_1(\sin x_i \cos b_2)^2 \\ & + 4b_1 \sin x_i \cos b_2 \cos x_i \sin b_2 + 2b_1(\cos x_i \sin b_2)^2 \end{aligned} \tag{F.16}$$

Replacing the values of x_i from the histogram (equation F.2) and separating equation F.16 in its different components:

$$\begin{aligned} \sum_{i=1}^{N} \sin^2 x_i \quad &= \quad \sum_{i=1}^{N} \sin^2(\frac{2\pi}{N} i) \;=\; \sum_{i=1}^{N} \frac{1 - \cos 2(\frac{2\pi}{N} i)}{2} = \frac{N}{2} \;-\; \frac{1}{2} \sum_{i=1}^{N} \cos 2(\frac{2\pi}{N} i) \\ &= \quad \frac{N}{2} \;-\; \frac{1}{2}(\sum_{i=1}^{\frac{N}{4}} \cos \frac{4\pi i}{N} i + \underbrace{\sum_{i=\frac{N}{4}+1}^{\frac{N}{2}}}_{k=i-\frac{N}{4}} \cos \frac{4\pi i}{N}) \\ & \quad -\frac{1}{2}(\sum_{i=\frac{N}{2}+1}^{\frac{3N}{4}} \cos \frac{4\pi i}{N} + \underbrace{\sum_{i=\frac{3N}{4}+1}^{N}}_{k=i-\frac{N}{4}} \cos \frac{4\pi i}{N}) \\ &= \quad \frac{N}{2} \;-\; \frac{1}{2}(\;0\;) \;-\; \frac{1}{2}(\;0\;) \;=\; \frac{N}{2} \end{aligned} \tag{F.17}$$

$$\sum_{i=1}^{N} \cos^2 x_i \quad = \quad \sum_{i=1}^{N} 1 \;-\sum_{i=1}^{N} \sin^2 x_i \;=\; N - \frac{N}{2} \;= \frac{N}{2} \tag{F.18}$$

$$\begin{aligned}
\sum_{i=1}^{N} \sin x_i \cos x_i &= \sum_{i=1}^{N} \sin(\frac{2\pi}{N} i) \cos(\frac{2\pi}{N} i) \\
&= \frac{1}{2} \sum_{i=1}^{N} \sin 2(\frac{2\pi}{N} i) \\
&= \frac{1}{2}(\sum_{i=1}^{\frac{N}{4}} \sin \frac{4\pi i}{N} i + \underbrace{\sum_{i=\frac{N}{4}+1}^{\frac{N}{2}}}_{k=i-\frac{N}{4}} \sin \frac{4\pi i}{N}) \\
&\quad -\frac{1}{2}(\sum_{i=\frac{N}{2}+1}^{\frac{3N}{4}} \sin \frac{4\pi i}{N} + \underbrace{\sum_{i=\frac{3N}{4}+1}^{N}}_{k=i-\frac{N}{4}} \sin \frac{4\pi i}{N}) \;=\; 0
\end{aligned} \tag{F.19}$$

Then equation F.16 is simply:

$$\begin{aligned}
0 \;=\; & -2\cos b_2 \sum_{i=1}^{N} \tilde{y}_i \sin x_i \; - 2\sin b_2 \sum_{i=1}^{N} \tilde{y}_i \cos x_i \\
& + 2b_1 \cos^2 b_2 (\frac{N}{2}) + 4b_1 \sin b_2 \cos b_2 (0) \; + 2b_1 \sin^2 b_2 (\frac{N}{2})
\end{aligned} \tag{F.20}$$

And finally:

$$b_1 = \frac{2}{N}(\cos b_2 \sum_{i=1}^{N} \tilde{y}_i \sin x_i + \sin b_2 \sum_{i=1}^{N} \tilde{y}_i \cos x_i) \tag{F.21}$$

Minimizing the expression F.13 using conditions F.4 and solving for b_2:

$$\sum_{i=1}^{N} 2(\tilde{y}_i - b_1 \sin(x_i + b_2))(-b_1 \cos(x_i + b_2)) = 0 \tag{F.22}$$

$$\begin{aligned} 0 &= \sum_{i=1}^{N} -2b_1\tilde{y}_i(\cos x_i \cos b_2 - \sin x_i \sin b_2) \\ &+ \sum_{i=1}^{N} 2b_1^2(\sin x_i \cos b_2 + \cos x_i \sin b_2)(\cos x_i \cos b_2 - \sin x_i \sin b_2) \end{aligned} \tag{F.23}$$

Takin into account the results from equations F.17 , F.18 and F.19:

$$\begin{aligned} \sum_{i=1}^{N} 2b_1^2(\sin x_i \cos b_2 + \cos x_i \sin b_2)(\cos x_i \cos b_2 - \sin x_i \sin b_2) &= -\, b_1^2 N \sin b_2 \cos b_2 \\ &+ b_1^2 N \sin b_2 \cos b_2 = 0 \end{aligned} \tag{F.24}$$

Therefore equation F.23 is simply:

$$-2b_1 \cos b_2 \sum_{i=1}^{N} \tilde{y}_i \cos x_i + 2b_1 \sin b_2 \sum_{i=1}^{N} \tilde{y}_i \sin x_i = 0 \tag{F.25}$$

$$\sin b_2 \sum_{i=1}^{N} \tilde{y}_i \sin x_i = \cos b_2 \sum_{i=1}^{N} \tilde{y}_i \cos x_i \tag{F.26}$$

$$b_2 = \arctan\left(\frac{\sum_{i=1}^{N} \tilde{y}_i \cos x_i}{\sum_{i=1}^{N} \tilde{y}_i \sin x_i}\right) \tag{F.27}$$

We can use result in equation F.27 to express b_1 in terms of the data:

$$\begin{aligned} b_1 &= \frac{2}{N}\left(\cos\left(\arctan \frac{\sum_{i=1}^{N} \tilde{y}_i \cos x_i}{\sum_{i=1}^{N} \tilde{y}_i \sin x_i}\right) \sum_{i=1}^{N} \tilde{y}_i \sin x_i \right. \\ &+ \left. \sin\left(\arctan \frac{\sum_{i=1}^{N} \tilde{y}_i \cos x_i}{\sum_{i=1}^{N} \tilde{y}_i \sin x_i}\right) \sum_{i=1}^{N} \tilde{y}_i \cos x_i \right) \end{aligned} \tag{F.28}$$

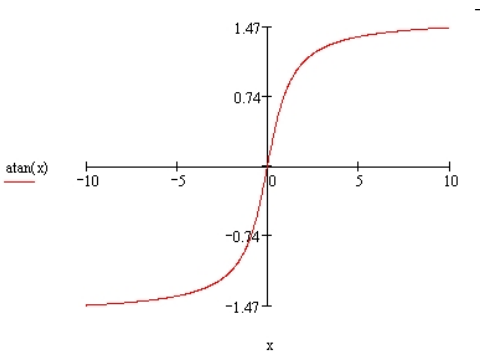

Figure F.1: Arctangent Function

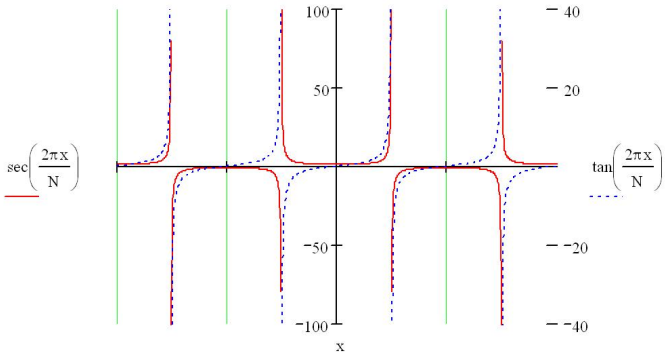

Figure F.2: Secant and Tangent Functions, indicating the expected amplitude and phase of the fitted sinusoidal

As seen in figure F.1 the value for b_2 is between $-\frac{\pi}{2}$ and $\frac{\pi}{2}$. The phase on the other hand should be expressed in values ranged from 0 to 2π for a sine function of positive amplitude.

For the first quadrant, the phase should be between 0 and $\pi/2$, but the value of the arctangent is between 0 and $-\pi/2$. For the second quadrant the phase should be between $\pi/2$ and π, but the value of the arctangent is between $\pi/2$ and 0. For the third quadrant the phase should be between π and $\frac{3\pi}{2}$, but the value of the arctangent is between 0 and $\pi/2$. For the forth quadrant the phase should be between $\frac{3\pi}{2}$ and 2π, but the value of the arctangent is between $-\pi/2$ and 0. The correction for the phase value is done by simply adding the proper constant value to the value of the arctangent. See figure F.2.

$Y(x)$ can be simplified greatly by taking the result in equation F.26 and replacing $\sum_{i=1}^{N}\ \tilde{y}_i \cos x_i$ in the general expression.

$$\begin{aligned} b_1 &= \frac{2}{N}(\cos b_2 \sum_{i=1}^{N} \tilde{y}_i \sin x_i + \frac{\sin^2 b_2}{\cos b_2} \sum_{i=1}^{N} \tilde{y}_i \sin x_i) \\ &= \frac{2}{N \cos b_2} \sum_{i=1}^{N} \tilde{y}_i \sin x_i (\cos^2 b_2 + \sin^2 b_2) \\ &= \frac{2}{N \cos b_2} \sum_{i=1}^{N} \tilde{y}_i \sin x_i \end{aligned} \tag{F.29}$$

$$\begin{aligned} Y(x) &= \frac{1}{N} \sum_{i=1}^{N}\ y_i + \frac{2}{N \cos b2} \sum_{i=1}^{N} \tilde{y}_i \sin x_i\ \ \sin(x + b_2) \\ &= \frac{1}{N} \sum_{i=1}^{N}\ y_i + \frac{2}{N \cos b2} \sum_{i=1}^{N} \tilde{y}_i \sin x_i\ (\sin x \cos b_2 + \cos x \sin b_2) \\ &= \frac{1}{N} \sum_{i=1}^{N}\ y_i + \frac{2}{N} \sin x \sum_{i=1}^{N} \tilde{y}_i \sin x_i\ + \frac{2}{N} \cos x \frac{\sin b_2}{\cos b2} \sum_{i=1}^{N} \tilde{y}_i \sin x_i \\ &= \frac{1}{N} \sum_{i=1}^{N}\ y_i + \frac{2}{N} \sin x \sum_{i=1}^{N} \tilde{y}_i \sin x_i \\ &+ \frac{2}{N} \cos x \tan(\arctan(\frac{\sum_{i=1}^{N}\ \tilde{y}_i \cos x_i}{\sum_{i=1}^{N}\ \tilde{y}_i \sin x_i})) \sum_{i=1}^{N} \tilde{y}_i \sin x_i \\ &= \frac{1}{N} \sum_{i=1}^{N}\ y_i + \frac{2}{N} \sin x \sum_{i=1}^{N} \tilde{y}_i \sin x_i\ + \frac{2}{N} \cos x \sum_{i=1}^{N} \tilde{y}_i \cos x_i \end{aligned} \tag{F.30}$$

Finally, the least-square function is of the form:

$$Y(x) = \bar{y} + (\frac{2}{N} \sum_{i=1}^{N} (y_i - \bar{y}) \sin x_i\ ) \sin x + (\frac{2}{N} \sum_{i=1}^{N} (y_i - \bar{y}) \cos x_i) \cos x \tag{F.31}$$

F.2 Analysis of variance

After fitting the level (b_0), amplitude (b_1) and phase (b_2) of the sinusoidal envelope to the N bins of the histogram, we use analysis of variance to test the significance of the regression.

To test the significance of the regression we compute $F_{\nu-1,n-\nu}$, where $\nu = 3$ and $n = 32$,

For the least squares fit:

$$\sum_{i=1}^{N} (y_i - \bar{y}_i)^2 = \sum_{i=1}^{N} (Y_i - \bar{y}_i)^2 + \sum_{i=1}^{N} (y_i - Y_i)^2 \tag{F.32}$$

$$\sum_{i=1}^{N} (\widetilde{y_i})^2 = \sum_{i=1}^{N} (b_1 \sin(x_i + b_2))^2 + \sum_{i=1}^{N} (\widetilde{y_i} - b_1 \sin(x_i + b_2))^2 \tag{F.33}$$

$$t_l = R_g + R_s \tag{F.34}$$

$$t_l = \sum_{i=1}^{N} (\widetilde{y_i})^2 \tag{F.35}$$

$$R_g = \sum_{i=1}^{N} (b_1(\sin x_i \cos b_2 + \cos x_i \sin b_2))^2 \tag{F.36}$$

$$R_g = \sum_{i=1}^{N} (b_1^2((\sin x_i \cos b_2)^2 + (\cos x_i \sin b_2)^2 + 2 \sin x_i \cos b_2 \cos x_i \sin b_2) \tag{F.37}$$

Takin into account the results from equations F.17 , F.18 and F.19:

$$R_g = (N/2)^3(b_1^2(\cos b_2^2 + \sin b_2^2) = (N/2)^3 b_1^2 \tag{F.38}$$

$$R_g = N/2(\cos b_2 \sum_{i=1}^{N} \tilde{y}_i \sin x_i + \sin b_2 \sum_{i=1}^{N} \tilde{y}_i \cos x_i)^2 \tag{F.39}$$

$$R_s = t_l - R_g \tag{F.40}$$

$$F_{2,29} = \frac{R_g/2}{R_s/29} \tag{F.41}$$

After fitting the amplitude and phase of a sinusoidal envelope to the 32 bins of the histogram using non-linear regression, we use analysis of variance to test the significance of the regression (see chapter 6). Assuming that the phase of the response is known (preserved from previous stimulus), and fitting the amplitude of a sinusoidal envelope to the 32 bins of the histogram using curvilinear regression, we use analysis of variance to test the significance of the regression (see chapter 6). The threshold of sensitivity is the last stimulus amplitude with both significant at the 5% level without reference ($P(F_{2,29} > 3.33) = 0.05$) and with the reference ($P(F_{1,30} > 4.17) = 0.05$).

Bibliography

[1] G. N. Akoev, P. M. Zhadan, O. B. Il'insky, and E. S. Titkov. Electrophysiological investigations of the properties of the electroreceptors (ampullae of lorenzini) in black sea rays. *Neurophysiology*, 6(4):426–433, July-August 1974.

[2] N. P. Antipin, B. V. Krylov, and V. L. Cherepnov. Topography of the ampullary system of raja clavata and its role in electroorientation. *Neurophysiology*, 16(6):628, 1985.

[3] A. Banos and J. P. Wesley. The horizontal electric dipole in a conducting half-space. SIO Reference 53-33, Scripps Institution of Oceanography, 1953.

[4] M. V. Bennett and W. T. Clusin. Transduction at electroreceptors: origins of sensitivity. *Society of General Physiologists series*, 33:91, 1979.

[5] G. R. Broun and V. I. Govardovskii. Electroreceptor mechanisms of the ampullae of lorenzini in skates. *Neurophysiology*, 15(2):178–185, 1983.

[6] G. R. Broun and V. I. Govardovskii. Electroreceptor model of the electroreceptor of the ampullae of lorenzini. *Neurophysiology*, 15(3):235–241, 1983.

[7] G. R. Broun, O. B. Il'inskii, and B. V. Krylov. Response of the ampullae of lorenzini in a uniform electric field. *Neurophysiology*, 11(2):158–166, 1979.

[8] W. T. Clusin and M. V. Bennett. Calcium-activated conductance in skate electroreceptors: current clamp experiments. *The Journal of General Physiology*, 69(2):121, 1977.

[9] D. A. Ebert. *Sharks, Rays, and Chimaeras of California.* University of California Press, 2003.

[10] M. Faraday. Experimental researches in electricity. second series. the bakerian lecture. 5. terrestrial magneto-electric induction. 6. force and direction of magneto-electric induction generally. *Philosophical Transactions of the Royal Society of London*, 122:163, 1832.

[11] R. D. Fields and M. H. Ellisman. Functionally significant plasticity of synaptic morphology: Studies on the ribbon synapse of the ampullae of lorenzini. *Neuroscience*, 25(2):705–720, 1988.

[12] R. D. Fields, M. H. Ellisman, and S. G. Waxman. Changes in synaptic morphology associated with presynaptic and postsynaptic activity: an in vitro study of the electrosensory organ of the thornback ray. *Synapse*, 1(4):335, 1987.

[13] L. Fishelson and A. Baranes. Disribution, morphology, and cytology of ampullae of lorenzini in the oman shark, iago omanensis (triakidae), from the gulf of aqaba, red sea. *The Anatomical Record*, 251:417–430, 1998.

[14] L. Goldstein. Volume regulation in the erythrocyte of the little skate, raja erinacea. *Journal of Experimental Zoology*, 252(s2):136, 1989.

[15] L. Goldstein and R. P. Forster. Osmoregulation and urea metabolism in the little skate raja erinacea. *American Journal of Physiology*, 220(3):742, 1971.

[16] J. D. Jackson. *Classical Electrodynamics*. John Wiley and Sons, 2 edition, 1975.

[17] A. J. Kalmijn. Electro-perception in sharks and rays. *Nature*, 212(5067):1232, 1966.

[18] A. J. Kalmijn. Bioelectric fields in sea water and the function of the ampullae in elasmobranch fishes. Technical report, CNRS and ZWO, translated by ONR, Laboratoire Arago, Banyuls-sur-Mer, France, 1969.

[19] A. J. Kalmijn. The electric sense of sharks and rays. *The Journal of Experimental Biology*, 55(2):371, 1971.

[20] A. J. Kalmijn. *Handbook of Sensory Physiology*, volume 3, chapter The Detection of Electric Fields from Inanimate and Animate Sources Other Than Electric Organs, page 46. Handbook of Sensory Physiology, 1974.

[21] A. J. Kalmijn. *Sensory Biology of Sharks, Skates, and Rays*, chapter Electric and Magnetic Sensory World of Sharks, Skates, and Rays, pages 507–528. Office of Naval Research, 1978.

[22] A. J. Kalmijn. Biophysics of geomagnetic-field detection. *IEEE Transactions on Magnetics*, 17(1):1113, 1981.

[23] A. J. Kalmijn. Orientation to uniform electric-fields in the stringray urolophus-halleri - sensitivity of response. *The Biological Bulletin*, 161(2):347, 1981.

[24] A. J. Kalmijn. Electric and magnetic-field detection in elasmobranch fishes. *Science*, 218(4575):916, 1982.

[25] A. J. Kalmijn. *Comparative Physiology of Sensory Systems*, chapter Theory of electromagnetic orientation: a further analysis, pages 525–560. Cambridge University Press, 1984.

[26] A. J. Kalmijn. *Sensory Biology of Aquatic Animals*, chapter Detection of Weak Electric Fields, pages 151–186. Springer-Verlag, 1987.

[27] A. J. Kalmijn. Detection and processing of electromagnetic and near-field acoustic signals in elasmobranch fishes. *Philosophical Transactions of the Royal Society of London. Series B, Biological sciences*, 355(1401):1135, 2000.

[28] A. J. Kalmijn. *Graded Positive Feedback in Elasmobranch Ampullae of Lorenzini.* CP665, Unsolved Problems of Noise and Fluctuations. American Institute of Physics, 2003.

[29] A. J. Kalmijn. *Sensory processing in aquatic environments*, volume 2, chapter Physical Principles of Electric, Magnetic, and Near-Field Acoustic Orientation. Springer New York, 2003.

[30] A. J. Kalmijn, I. F. Gonzalez, and M. C. McClune. The physical nature of life. *Journal of Physiology, Paris*, 96(5-6):355–362, Sep-Dec 2002.

[31] M. Kantner, W. F. Knig, and W. Reinbach. Bau und innervation der lorenzinischen ampullen und deren bedeutung als niederes sinnesorgan. *Cell and Tissue Research*, 57(1):124, 1962.

[32] E. I. Knudse. Spatial aspects of the electric fields generated by weakly electric fish. *Journal of Comparative Physiology*, 99:103, 1975.

[33] M. S. Longuet-Higgins, M. E. Stern, and H. M. Stommel. The electrical field induced by ocean currents and movements. *Papers in Physical Oceanography and Meteorology*, III:34, 1954.

[34] J. Lu and H. M. Fishman. Localization and function of the electrical oscillation in electroreceptive ampullary epithelium from skates. *Biophysical Journal*, 69(6):2458, 1995.

[35] R. P. Malchow and H. Ripps. Effects of gamma-aminobutyric acid on skate retinal horizontal cells: Evidence for an electrogenic uptake mechanism. *Proceedings of the National Academy of Sciences of the United States of America*, 87(22):8945, 1990.

[36] H. E. Metcalf. The innervation of the ampullae of lorenzini in acanthias vulgaris. *Transactions of American Microscopical Society*, 35(2), April 1916.

[37] J. C. Montgomery. Noise cancellation in the electrosensory system of the thornback ray common mode rejection of input produced by the animal's own ventilatory movement. *Journal of Comparative Physiology. A, Sensory, Neural, and Behavioral Physiology*, 155(1):103, 1984.

[38] R. W. Murray. The response of the ampullae of lorenzini of elasmobranchs to mechanical stimulation. *The Journal of Experimental Biology*, 37(2):417, 1960.

[39] R. W. Murray. Response of ampullae of lorenzini of elasmobranchs to electrical stimulation. *The Journal of Experimental Biology*, 39(1):119, 1962.

[40] R. W. Murray. Electroreceptor mechanisms:the relation of impulse frequecy to stimulus strenght and responses to pulsed stimuli in the ampullae of lorenzini of elasmobranchi. *The Journal of Physiology*, 180:592–606, 1965.

[41] H. W. Norris. The laterosensory system of torpedo marmorata, innervation, and morphology. *Journal of Comparative Neurology*, 56(1):169, 1932.

[42] J. E. Peabody. The ampullae of lorenzini of the selachii. *Zoological Bulletin*, 1(4):163–178, December 1897.

[43] W. Raschi. A morphological analysis of the ampullae of lorenzini in selected skates (pisces, rajoidei). *Journal of Morphology*, 189(3):225, 1986.

[44] A. Sand. The function of the ampullae of lorenzini, with some observations on the effect of temperature on sensory rhythms. *Proceedings of the Royal Society of London*, 125(841):524, 1938.

[45] T. B. Sanford. Measurements by geomagnetic induction of volume transport in a salt marsh drainage channel. *Limnology and Oceanography*, 22(5):1082–1089, 1977.

[46] T. J. Sejnowski and M. L. Yodlowski. A freeze-fracture study of the skate electroreceptor. *Journal of Neurocytology*, 11, 1982.

[47] K. Umashankar. *Introduction to Engineering Electromagnetic Fields*, volume 4 of *Advanced Series in Electrical and Computer Engeneering*. World Scientific, 1989.

[48] M. R. Urist. Calcium and phosphorus in the blood and skeleton of the elasmobranchii. *Endocrinology*, 69:778, 1961.

[49] W. Von Arx and H. Stommel. Second report on the geomagnetic electrokinetograph and the theory of the electric potential field induced in deep ocean currents. Technical report, WHOI, Massachusetts, 1948.

[50] J. R. Wait. The electromagnetic fields of a horizontal dipole in the presence of a conducting half-space. *Canadian Journal of Physics*, 39:1017–1028, 1961.

[51] B. Waltman. Electrical properties and fine structure of ampullary canals of lorenzini. *Acta Physiologica Scandinavica*, S 66:3, 1966.